LAWRENCE
LIVERMORE
NATIONAL
LABORATORY

LLNL-JRNL-413271

Spectral shifts and helium configurations in 4HeN-tetracene clusters

H. D. Whitley, J. L. DuBois, K. B. Whaley

May 22, 2009

Journal of Chemical Physics

Disclaimer

Spectral shifts and helium configurations in ^4He_N-tetracene clusters

Heather D. Whitley,[1,2], Jonathan L. DuBois,[1,2] and K. Birgitta Whaley[1]

[1] *Department of Chemistry and Kenneth S. Pitzer Center for Theoretical Chemistry, University of California, Berkeley, CA 94720*

[2] *Lawrence Livermore National Laboratory, Livermore, CA 94550*

(Dated: June 19, 2009)

Abstract

Spectral shifts of electronic transitions of tetracene in helium droplets are investigated in a theoretical study of ^4He_N-tetracene clusters with $1 \leq N \leq 150$. Utilizing a pair-wise interaction for the S_0 state of tetracene with helium that is extended by semi-empirical terms to construct a potential for the S_1 state of tetracene with helium, the spectral shift is calculated from path integral Monte Carlo calculations of the helium equilibrium properties with tetracene in the S_0 and S_1 states at $T = 0$ and at $T = 0.625$ K. The calculated spectral shifts are in quantitative agreement with available experimental measurements for small values of N (≤ 8) at T$\sim$ 0.4 K and show qualitative agreement for larger N (10 - 20). The extrapolated value of the spectral shift in large droplets ($N \sim 10^4$) is $\sim 90\%$ of the experimentally measured value. We find no evidence of multiple configurations of helium for any cluster size, for both the S_0 or S_1 states of tetracene. These results suggest that the observed spectral splitting of electronic transitions of tetracene in large helium droplets is not due to co-existence of static meta-stable helium densities, unlike the situation previously analyzed for the phthalocyanine molecule.

PACS numbers: 36.40.Mr,61.46.-w,67.25.bh

I. INTRODUCTION

The utility of superfluid helium droplets as an ultracold, gentle quantum matrix for single molecule spectroscopy has long been established.[1–3] Helium droplets have been utilized in experiments including ro-vibrational spectroscopy of linear and high symmetry molecules, electronic spectroscopy of various organic molecules, and photoelectron spectroscopy of pure and doped droplets. The high-resolution spectra of molecules in helium droplets not only provide insight into the molecular characteristics, but also provide information regarding the characteristics of superfluid helium in a nanoscale system. Clusters of a small number of He atoms with embedded molecules offer information on how the microscopic delocalization of helium atoms evolves into nanoscale superfluidity [4].

The electronic spectra of molecules in helium droplets consist of sharp features, corresponding to the vibronic transitions of the dopant molecule, accompanied by broad features to the blue of the sharp lines. These broad features correspond to the coupling of excitations of the phonon modes of the helium droplet to the electronic excitation of the molecule. One class of spectra which has been extensively studied in helium droplets is the electronic spectra of planar aromatic molecules, or PAMs.[5–23] These molecules are interesting, not only due to their practical and biological relevance, but also because they represent nanoscale precursors to bulk graphite, enabling the study of quantum adsorption in the nanoscale size regime. The spectra of these molecules in ^{4}He droplets often exhibit anomalous characteristics, including sharp lines in the phonon wings, as well as split vibronic peaks in both absorption and emission spectra. Several theoretical investigations of these spectral features have also been conducted.[24–29]

One of the most well-studied PAMs in helium droplets is the tetracene molecule.[5–13, 26, 28] One motivating factor for this proliferation of experimental studies is the observation of an anomalous splitting of the zero-phonon line (ZPL) in its absorption spectrum. This was first measured by laser-induced fluorescence (LIF) in 1998 by Hartmann *et al.* for droplets with $N \sim 6000$ helium atoms, where it was observed that the purely vibronic lines are split by ~ 1 cm^{-1}, with a red-shift of 103.1 cm^{-1} relative to the bare molecule.[5] Splitting is not observed in the electronic spectra of tetracene clusters with other rare gas atoms. It has therefore been attributed as a unique feature of the He quantum solvation environment. The two lines in the split ZPL are termed the α and β lines; the structureless α line lies

to the red of the structured β line.[11] The assignment of spectral transitions as α-type or β-type in studies of tetracene is therefore made according to whether the transitions exhibit fine structure or are structureless. The fine structure of the β band has been tentatively assigned to rotational excitations of the molecule which are coupled to the excitations of the first shell of helium.[11] The splitting of the ZPL is much larger than what would be expected for resolved rotational structure, and has been viewed as a characteristic that is a consequence of the unique nature of helium. Previous proposals for the origin of the ZPL splitting include different configurations of helium near the tetracene molecule, or a 'tunneling' type of excitation of one or more atoms adsorbed in the double-well-like part of the He-tetracene potential energy surface, above and below the central rings.[7]

In this paper we investigate whether the spectral splitting of tetracene is due to the existence of multiple solvation configurations of helium around the molecule. We perform path integral Monte Carlo simulations of He_N-tetracene clusters with N ranging from 1 to 150 atoms, in which the tetracene molecule is treated as a stationary rigid body. Calculations are made using both the $T = 0$ Variational Path Integral (VPI) method and the finite temperature approach with $T = 0.625$ K, for both the S_0 and S_1 electronic states of the tetracene molecule. For the interaction potential of the molecule in the S_0 state with helium we employ a pairwise atomic sum. For the interaction of the S_1 state with helium we use the same type of semi-empirical interaction potential as that employed in our previous study of phthalocyanine,[27] but with a greater accuracy here that is afforded by the ability to determine the semi-empirical parameters by fitting to experimental spectral shift data for small He-tetracene clusters with $N \leq 17$.[6] The resulting helium configurations show that up to three helium atoms are strongly localized on the surface of the tetracene molecule, oriented along the long axis. Our results do not show any evidence for the existence of multiple helium solvation configurations at these temperatures. The spectral shift values for small cluster sizes ($N \leq 17$) are in reasonable agreement with those measured in size-specific clusters formed by tetracene collisions with cold helium gas.[6] The calculated spectral shift increases with N, reaching a value of $\sim$-84 cm^{-1} at $N = 150$. Our results do not support the presence of multiple static meta-stable He configurations. We therefore conclude that the observed splitting of the tetracene ZPL in He droplets is instead the result of the dynamical characteristics of the helium localized near the molecule. This will be investigated in a future publication.[30]

II. THEORY AND COMPUTATIONAL METHODS

Electronic spectra of tetracene and other molecules in ^{4}He clusters show shifts of the band origins that are due to interactions between the molecule and its solvating helium environment. These interactions shift the energies of both the ground and electronically excited states of the molecule. Calculating the spectral shift therefore requires accurate information about the He-molecule interactions with the molecule in both the ground and the relevant excited electronic states. In this work we perform simulations of $^4\mathrm{He}_N$-tetracene clusters in the S_0 and S_1 molecular states, using corresponding electronic state-specific interaction potentials. We utilize the finite-temperature path integral Monte Carlo (PIMC) method to study He-tetracene clusters at $T = 0.625$ K, as well as ground state variational path integral Monte Carlo (VPI) for $T = 0$ K calculations. The molecule is treated as a stationary rigid body. Given the much larger mass of the tetracene molecule relative to a helium atom, it is reasonable to neglect the translational and rotational motion of the molecule, while at these low temperatures we may also neglect the molecular vibrational degrees of freedom. For clusters studied via VPI, we calculate the spectral shift of the electronic origin from the difference in the ground state energies of helium in the adiabatic S_0 and S_1 interaction potentials.[31]

A. Hamiltonian and interaction potentials

Tetracene, $C_{18}H_{12}$, is a planar aromatic molecule with D_{2h} molecular symmetry. In this study, we use the typical benzene coordinates ($r_{\mathrm{C-C}} = 1.40$ Å and $r_{\mathrm{C-H}} = 1.08$ Å) to generate the tetracene atom coordinates. In our present calculations, the tetracene molecule is held static at the origin in the xy plane during the course of the simulation since its large mass relative to helium ensures negligible contribution of the molecular translational motion to the energies and other quantities of interest. The Hamiltonian for the systems studied here is

$$\hat{H} = -D_4 \sum_{i=1}^{N} \hat{\nabla}_i^2 + \hat{V}, \tag{1}$$

where the first term is the total helium kinetic energy, with $D_4 \equiv \frac{\hbar^2}{2m_{\mathrm{He}}}$, and $\hat{V}$ contains terms for both He-He and He-tetracene interactions. This is an N-body Hamiltonian for the helium atoms, with the He-tetracene interaction playing the role of an external potential.

For tetracene in the S_0 state, the system interaction potential is a simple sum over two-body interactions:

$$V_{S_0} = \sum_{j=1}^{N} V_{\mathrm{I}}(\mathbf{r}_j) + \sum_{i<j}^{N} V_{\mathrm{He}}(|\mathbf{r}_j - \mathbf{r}_i|). \tag{2}$$

Here V_{He} is the widely-used Aziz potential for helium[32] and the He-tetracene potential is defined as a sum of He-C and He-H Lennard-Jones interactions,

$$V_{\mathrm{I}}(\mathbf{r}) = \sum_{\alpha} 4\epsilon_\alpha \left[\left(\frac{\sigma_\alpha}{|\mathbf{r} - \mathbf{r}_\alpha|} \right)^{12} - \left(\frac{\sigma_\alpha}{|\mathbf{r} - \mathbf{r}_\alpha|} \right)^{6} \right], \tag{3}$$

where the index α goes over all individual C and H atoms of the molecule. The Lennard-Jones parameters used in this study are the same as those used in our previous studies of PAMs in the S_0 state and are given in Table I.[26, 27] The parameters for the He-C interaction were derived from scattering data of helium at a graphite surface,[33] while those for the He-H interaction were determined by low energy elastic scattering of helium and hydrogen atoms.[34] The He-tetracene interaction potential for the S_0 state is shown in panel a) of Fig. 1. The predominant features of this potential energy surface are four minima located near the center of each aromatic ring on each side of the molecule. The two inner minima are the global minima of the potential (~ -115 cm^{-1}), while the outer minima lie slightly higher in energy (~ -106 cm^{-1}). For analysis of the helium configurations we shall focus on the attractive region above the surface of the carbon skeleton of the tetracene molecule, namely the region defined by -1.0 Å $\leq y \leq 1.0$ Å and -5.0 Å$\leq x \leq 5.0$ Å, for a given perpendicular distance z from the molecule.

Theoretical investigation of clusters involving molecules in their S_1 states has typically been limited by a lack of suitable interaction potentials. A method for approximating the interaction potential of a rare gas atom with a planar aromatic molecule in the S_1 state was previously derived and successfully utilized by Shalev *et al.* to describe clusters of PAMs with Ne, Ar, Kr, and Xe.[35] In this method, the change in the purely attractive dispersive interaction of the rare gas atom with the excited molecule, V_{DSS}, is derived from second-order perturbation theory and then added to the S_0 interaction potential in order to generate an interaction potential for the S_1 excited state. This typically includes a scaling factor that is determined by fitting the calculated spectral shift for a rare gas atom-molecule dimer to the corresponding experimentally measured shift. In subsequent applications to clusters of PAMs with the lighter He atom, Heidenreich *et al.* found that it is also necessary to account

for a change in the repulsive interactions between He and the PAM and demonstrated that this change can be treated by semi-empirically scaling the Lennard-Jones σ parameter for He-C interactions.[36, 37] Thus for helium-PAM interactions, experimental data from the dimer species is needed in order to fit both attractive and repulsive scaling parameters. The scaling factor for the attractive terms has only a weak dependence on the rare gas species,[35] so that the He attractive scaling factor can, in the absence of any experimental data, be estimated from e.g., the corresponding scaling factor for Ar. However, this approach precludes the incorporation of any change in repulsive interactions in the S_1 state. This was necessarily the situation for the He-phthalocyanine interaction potential that was used in our previous study of phthalocyanine-helium clusters [27]. For tetracene, a better approach is possible since electronic spectra have been measured for clusters with small numbers of helium atoms ($N = 1 - 17$) and the observed shifts for the $N = 1$ "dimer" cluster may be then used to make the required empirical fits of all scaling parameters. Therefore, in the present study we include both the dispersive and repulsive changes in the S_1 interaction potential for He-tetracene:

$$V_{S_1} = V_{S_0} + V_{\rm DSS} + \Delta V_{\rm LJ} \tag{4}$$

where [35]

$$V_{\rm DSS} = -\eta \left(\frac{e^2}{2}\right) \alpha_A \bar{F} \sum_{l=1}^{\rm N} \sum_{\alpha,\alpha'} S^{(l)}_{\alpha\alpha'} G_{\alpha\alpha'}, \tag{5}$$

and [36]

$$\Delta V_{\rm LJ} = \sum_{i=1}^{N} \sum_{\gamma} 4\epsilon \frac{\sigma_{\rm ex}^{12} - \sigma^{12}}{|\mathbf{r}_i - \mathbf{r}_\gamma|^{12}}. \tag{6}$$

Note that Eq. (5) includes three-body terms, corresponding to atom α–helium l–atom α' interactions, where l denotes a He atom and α and α' denote two possibly different atoms in the tetracene molecule. Here α_A is the static polarizability of the helium atom and $\bar{F}$ is its ionization energy, $S^{(l)}_{\alpha\alpha'}$ is a geometric factor for the two or three body interactions of helium atom, l, with carbon atoms α and α', and $G_{\alpha\alpha'}$ is the electronic factor accounting for the transition monopoles on atoms α and α' in the molecule.[35] The parameter η corrects for the overestimation of the oscillator strength of π-π^* transitions, $G_{\alpha,\alpha'}$, that results from the simple Hückel molecular orbital theory used in the approach of Ref. 35. The parameter $\sigma_{\rm ex}$ in Eq. 6 is the scaling parameter for the repulsive component of the Lennard-Jones potential with the carbon atoms in the 9, 10, 11 and 12 positions in the tetracene molecule (we use

the numbering convention of Ref. 38). We do not modify the interactions between helium and hydrogen atoms in the S_1 state, since the π-π^* transition does not significantly modify the electron density near the hydrogen atoms.

In order to determine the semi-empirical parameters η and $\sigma_{\rm ex}$, we performed a series of path integral Monte Carlo simulations for the $N = 1$ "dimer" cluster and tuned these parameters to fit the resulting spectral shift to the experimental value.[6] The resulting optimized values of η and $\sigma_{\rm ex}$ used in this study, as well as other relevant constants for the S_1 potential, are given in Table II. The S_1 potential is overall quite similar to the S_0 potential, with two global minima of $\sim$ -117 cm^{-1} that are located near the centers of the two central aromatic rings, as shown in panel b) of Fig. 1. Fig. 1c) shows the difference potential $\Delta V = V_{S_1} - V_{S_0}$. The difference potential is positive near the carbon atoms in the 9, 10, 11, and 12 positions as a result of incorporating the repulsive term ΔV_{LJ} into the helium interaction with tetracene in the S_1 state, in addition to the usual dispersive term.

B. Computational methods

The variational path integral method[39, 40] (VPI) is used here to investigate the ground state properties of helium near tetracene in both the S_0 and S_1 states for clusters with up to $N = 14$ helium atoms. The VPI method is similar to the more commonly utilized diffusion Monte Carlo (DMC) method in that both methods use imaginary time propagation of a trial wavefunction to find the ground state properties of the system of interest. For sufficiently long propagation in imaginary time, both methods yield exact expectation values for certain ground state properties. In contrast to the DMC method, quantities which are derived from operators which commute with the *position* operator, such as the density and the potential energy, are free of trial function bias in the VPI method, and thus correspond to exact ground state quantities when the propagation is carried out for sufficiently long imaginary times. In the DMC method, quantities which commute with the system Hamiltonian can be calculated exactly.

The application of the VPI method to liquid helium was studied in detail by Cuervo *et al.*.[40] who found that it can yield lower ground state energies than DMC in cases where the trial wavefunction is of low quality, due to the reduced influence of the trial wavefunction in VPI calculations. This method is therefore an ideal complement to our

previous DMC approach [26] for the study of planar aromatics, where the helium atoms are strongly localized and defining a trial wavefunction can be problematic.[41] Implementation of the VPI method entails sampling paths in imaginary time according to the probability density

$$\mathcal{P}(X) \propto \Psi_T(R_0)\Psi_T(R_M) \left\{ \prod_{j=0}^{M-1} G_0(R_j, R_{j+1}; \Delta\tau) \right\}, \tag{7}$$

where X represents the coordinates, $\{R\}$, of all N particles in the cluster for all M points in the discretized path, Ψ_T is a trial wavefunction evaluated at R_0 and R_M which are the coordinates at the endpoints of the path, and G_0 is the short-time Green's function. Similar to the finite-temperature path integral approach, the Green's function is discretized by factorization in imaginary time: $\exp[-\beta\hat{H}] = (\exp[-\Delta\tau\hat{H}])^M$, where $\beta = M\Delta\tau$ is the total length of the path and $\Delta\tau$ is the imaginary time step. In the limit $\beta \to \infty$, the distribution of walkers at the center of the path should be independent of the endpoints.

Due to the noncommutivity of the kinetic and potential energy operators, the Green's function is not exactly known, and an approximate form of the Green's function must be utilized. In the simplest 'primitive approximation' [42] the error is proportional to $(\Delta\tau)^2$ (to $(\Delta\tau)^3$ if the split operator form is used), necessitating the use of a very small time step, and thus many points along the imaginary time path. Increasing the number of points in the path leads to a dramatic increase in the computational expense of a VPI calculation, particularly when many particles are present in the system. Chin has shown how to use a larger imaginary time step by utilizing higher-order factorizations of the of the short-time Green's function [43]. Here, we use the fourth-order expansion of Ref. 43 that was also employed in [40]:

$$G_0(R_j, R_{j+1}; \Delta\tau) = \rho_F(R_j, R_{j+1}) \exp\left[-\frac{2\Delta\tau V(R_j)}{3}\right] \rho_V(R_j) \tag{8}$$

where

$$\rho_V(R_j) = \exp\left[-\frac{2\Delta\tau V(R_j)}{3} - \frac{(\Delta\tau)^3\hbar^2}{9m} \sum_{i=1}^{N} [\nabla_i V(R_j)]^2\right] \tag{9}$$

for odd values of j and $\rho_V(R_j) = 1$ otherwise, and $\rho_F(R_j, R_{j+1})$ is the free-particle propagator,

$$\rho_F(R, R'; \Delta\tau) = (4\pi D_4 \Delta\tau)^{-3N/2} \prod_{i=1}^{N} \exp\left[-\frac{|\mathbf{r}_i - \mathbf{r}_i'|^2}{4D_4\Delta\tau}\right]. \tag{10}$$

In the limit $\Delta\tau \to 0$ and $\beta \to \infty$, the probability density is equal to the square of the true ground state distribution, $|\psi_0(R_{M/2})|^2$, for any chosen trial function Ψ_T that is not

orthogonal to the true ground state. In the case of bosons, the ground state wavefunction is symmetric with respect to particle exchange, so choosing a trial function that meets this criterion is straightforward. It is therefore possible to calculate unbiased averages by taking an average with respect to the configurations at the midpoint of the path. For operators $\hat{O}$ that are diagonal in the position representation, such as the density operator, the expectation value is represented by a simple average over the midpoint configurations that are sampled according to $\mathcal{P}(X)$. The Metropolis sampling method guarantees that the configurations are sampled according to the Green's function [44, 45]. Therefore, for an ergodic system in the limit of a large number of samples, P,

$$\langle\psi_0|\hat{O}|\psi_0\rangle = \frac{1}{P}\sum_{i=1}^{P} O(R^i_{M/2}). \tag{11}$$

The Hamiltonian, however, is not diagonal in the position representation. The two most common methods to compute the total ground state energy in a VPI calculation are i) to calculate a 'mixed estimate' based on the trial wavefunction and the configuration at either of the two endpoints of the sampled paths ($k = 0$ or $k = M$),

$$\langle\psi_0|\hat{H}|\Psi_T\rangle = \frac{1}{P}\sum_{i=1}^{P} \Psi_T(R^i_k)^{-1}\hat{H}\Psi_T(R^i_k) \approx \langle\psi_0|\hat{H}|\psi_0\rangle, \tag{12}$$

and ii) to use the thermodynamic expression for the total energy.[42] For operators which commute with the Green's function, such as the Hamiltonian, the mixed estimate provides unbiased values of the ground state properties.[39] In this work we utilize the mixed estimate to evaluate the total energy.

The efficiency of the VPI approach can be improved by choosing a reasonable form of the trial wavefunction, thereby decreasing the length of the path necessary for convergence to the ground state. The trial functions used in our VPI study are products of two-body factors,

$$\Psi_T = \prod_{j=1}^{N} e^{-t_{\mathrm{I}}(\mathbf{r}_j)} \prod_{i<j}^{N} e^{-t_{\mathrm{He}}(|\mathbf{r}_j-\mathbf{r}_i|)} \tag{13}$$

where t_{I} and t_{He} describe helium-tetracene and helium-helium correlations, respectively:

$$t_{\mathrm{I}}(\mathbf{r}) = \sum_{\alpha}\left(\frac{c_\alpha}{|\mathbf{r}-\mathbf{r}_\alpha|}\right)^5 + ax^2 + by^2 + cz^2, \quad t_{\mathrm{He}}(r) = \left(\frac{c_{\mathrm{He}}}{r}\right)^5. \tag{14}$$

The variational parameters $c_\alpha, c_{\mathrm{He}}, a, b, c$ for clusters with $N < 8$ atoms were obtained by minimizing the variational energy of $\hat{H}$ with respect to Ψ_T.[41] For larger clusters, we modified the variational parameters in order to extend the range within which Ψ_T is nonzero. In

our VPI studies, we used inverse time steps of τ^{-1}/k_b =1000 to 2000 K with paths containing 514 to 1014 slices.

While we found that the VPI method worked well for clusters with $N \leq 14$, for larger clusters it was difficult to find high-quality trial wavefunctions, owing to the strong inhomogeneity of the He density in the He-tetracene system. Having a poor trial wavefunction slows convergence, necessitating the use of longer paths, which makes the calculations less efficient. We have therefore utilized the finite-temperature path integral Monte Carlo (PIMC)[46] approach to investigate larger clusters with up to $N = 150$ helium atoms. These calculations are made at $T = 0.625$ K and we assess the effect of finite temperature by comparing results from VPI and PIMC calculations for the small clusters.

In the PIMC method the equilibrium properties of a quantum system are computed from integrals over the thermal density matrix $\rho(\mathbf{R}, \mathbf{R}'; \beta) = \langle \mathbf{R}|e^{-\beta H}|\mathbf{R}'\rangle$:

$$\langle \hat{O} \rangle = \frac{1}{Z} \int d\mathbf{R} d\mathbf{R}' \langle \mathbf{R}'|\hat{O}|\mathbf{R}\rangle \rho(\mathbf{R}, \mathbf{R}'; \beta), \tag{15}$$

where $\beta = 1/k_B T$, $\mathbf{R}$ is a vector of the $3N$ coordinates for an N-body system and Z is the partition function. In order to incorporate the Bose statistics, the helium density matrix must be symmetrized for particle exchanges by summing over all N-particle permutations, $\mathcal{P}$:

$$\rho(\mathbf{R}, \mathbf{R}'; \beta) = \frac{1}{N!} \sum_{\mathcal{P}} \rho(\mathbf{R}, \mathcal{P}\mathbf{R}'; \beta). \tag{16}$$

In the discrete path integral formulation, the thermal density matrix, $\rho(\mathbf{R}, \mathcal{P}\mathbf{R}'; \beta)$, is replaced by a product of M high-temperature density matrices evaluated at temperature MT, corresponding to an imaginary time step $\tau = \beta/M$ between successive discrete integrations:

$$\begin{aligned} \rho(\mathbf{R}, \mathcal{P}\mathbf{R}'; \beta) \; = \; & \int \dots \int d\mathbf{R}_1 d\mathbf{R}_2 \dots d\mathbf{R}_{M-1} \rho(\mathbf{R}, \mathbf{R}_1; \tau) \\ & \times \rho(\mathbf{R}_1, \mathbf{R}_2; \tau) \dots \rho(\mathbf{R}_{M-1}, \mathcal{P}\mathbf{R}'; \tau). \end{aligned} \tag{17}$$

When the temperature MT is sufficiently high, the density matrix can be factored into the product of a free-particle propagator and an interaction term. A more complete description of this factorization and the accompanying convergence issues for pure helium systems is given in Ref. 42. In this study, we use the pair-product form of the exact two-body density matrix for all two-body interaction terms. In simulations within the S_1 state of tetracene, we split the sum in Eq. 5 into two sets of terms, namely those for which $\alpha = \alpha'$ and those for

which $\alpha \neq \alpha'$. The two-body terms where $\alpha = \alpha'$ are incorporated into the exact two-body density matrix. The remaining three-body terms for which $\alpha \neq \alpha'$ are treated within the lowest order primitive approximation, namely a simple Trotter factorization of the thermal density matrix with no further refinement.[42] A more detailed description of the PIMC implementation for molecules in helium can be found in Refs. 47 and 48. The primary limitation to the accuracy of our factorization of the thermal density matrix in this study is the treatment of the three-body terms in $V_{\rm DSS}$ within the primitive approximation. We find that an inverse time step of $\tau^{-1}/k_B \geq 80$ K yields converged He densities for both electronic states. Further reduction of the time step results in reduction of the total energy by ≤ 2 %, which we regard as an additional sign of good convergence. All PIMC calculations in this study were therefore carried out using $\tau^{-1}/k_B = 80$ K.

C. Spectral shift of electronic absorption spectra

Within the electric dipole approximation, the spectral density for excitations of the He-tetracene cluster can be calculated from the electric dipole correlation function [49]

$$A(\omega) \;=\; \int dt e^{i\omega t} \langle \mu(t)\mu(0)\rangle, \tag{18}$$

where

$$\begin{aligned} \langle \mu(t)\mu(0)\rangle \;&\equiv\; \mathrm{Tr}\left[\hat{\rho}\hat{\mu}(t)\hat{\mu}(0)\right] \\ &=\; \sum_k \langle \Psi_k|\rho\mu(t)\mu(0)|\Psi_k\rangle. \end{aligned} \tag{19}$$

Here μ is the molecular electronic transition dipole moment, $\{|\Psi_k\rangle\}$ are the eigenvectors of the full cluster Hamiltonian, which is given by sum of the N-body helium Hamiltonian Eq. (1) and the internal molecular electronic Hamiltonian, and $\hat{\rho} = \sum_i p_i |\Psi_i\rangle\langle\Psi_i|$ is the full cluster density operator. Inserting this into Eq. (19)

$$\langle \mu(t)\mu(0)\rangle \;=\; \sum_k \langle \Psi_k| \sum_i p_i |\Psi_i\rangle\langle\Psi_i|\mu(t)\mu(0)|\Psi_k\rangle. \tag{20}$$

and making use of completeness leads to

$$\begin{aligned} \langle \mu(t)\mu(0)\rangle \;&=\; \sum_i p_i e^{iE_i t}\langle\Psi_i|\mu \sum_j e^{-iE_j t}|\Psi_j\rangle\langle\Psi_j|\mu|\Psi_i\rangle \\ &=\; \sum_{ij} p_i e^{-i(E_j - E_i)t} |\langle\Psi_i|\mu|\Psi_j\rangle|^2. \end{aligned} \tag{21}$$

Due to the relatively weak interaction of helium with a molecule, the state of the full system can be approximately written as a product of a particular vibronic state of the molecule, $|\psi_e\rangle$, and the state of the N helium atoms, $|\Phi\rangle$, where the helium states are eigenfunctions of the N-body Hamiltonian, Eq. (1). We restrict our attention here to the pure electronic transitions between S_0 and S_1: for the case of the tetracene absorption spectrum there are then only two relevant molecular states, $|\psi_0\rangle$ and $|\psi_1\rangle$. Under the Born-Oppenheimer approximation, the dipole correlation function for the He-tetracene system can then be factorized as

$$\langle\mu(t)\mu(0)\rangle = \sum_{ij} p_i e^{-it(E_{1j}-E_{0i})} |\langle\psi_1|\mu|\psi_0\rangle|^2 |\langle\Phi_j^1|\Phi_i^0\rangle|^2, \tag{22}$$

where the superscripts on the N-body eigenfunctions of the helium atoms indicate the S_0 and S_1 states. The intensity of a transition in the He-tetracene cluster is therefore proportional to $|\langle\psi_1|\mu|\psi_0\rangle|^2|\langle\Phi_j^1|\Phi_i^0\rangle|^2$, where the second factor, the overlap of the final and initial helium N-body states, is a generalized Franck-Condon factor. Eq. (22) shows that the energy of a transition must be equal to the difference in the total energy of the cluster in the final and initial states, $E_{1j} - E_{0i}$. The $S_0 \rightarrow S_1$ spectrum therefore includes contributions from all transitions for which $|\langle\Phi_j^1|\Phi_i^0\rangle|^2 \neq 0$ and $p_i \neq 0$, and the transition energy between specific eigenstates, $E_{1j} - E_{0i} = \Delta E_{S_0 \rightarrow S_1} + \Delta E_{ij}$, is shifted by an amount $\Delta\nu = \Delta E_{ij}$ relative to the corresponding gas phase molecular transition $\Delta E_{S_0 \rightarrow S_1}$. A complete spectral calculation for a He-molecule cluster therefore requires determination of all He eigenstates with the molecule, in both S_0 and S_1 electronic states. We evaluate the spectral shift within three different approximations to Eq. (22).

1. Zero temperature shift

Previous studies of the vibrational energies of helium atoms on the surface of planar aromatic molecules find He excitations in the range of several wavenumbers.[23, 26, 37] Since spectroscopic measurements of molecules in helium droplets are made at temperatures of about 0.4 K [50], the spectral shift of the zero phonon transition of a planar aromatic molecule in helium can be assumed to be derived from transitions originating in the ground helium vibrational state for S_0. Due to the similarity of the S_0 and S_1 He-tetracene interactions, we expect that the He eigenfunctions for tetracene in S_1 are similar to those for

tetracene in S_0, which implies that transitions with $i = j$ will have the highest Franck-Condon factors. Under these assumptions, the shift of the ZPL will correspond to the difference in the He ground state energies in S_0 and S_1, i.e., $\Delta\nu = E_{10} - E_{00}$. In our zero temperature spectral shift calculation we therefore calculate the spectral shift of the ZPL for a cluster of a given size as the difference in the ground state energies from VPI calculations in S_0 and in S_1.

2. Perturbative estimates of zero temperature shift

If the helium wavefunctions are similar for tetracene in the two electronic states S_0 and S_1, it is reasonable to also investigate the use of a perturbative estimate of the spectral shift of the ZPL. Such perturbative estimates have been made for vibrational shifts of linear molecules [31, 51, 52], which are typically less than a few wavenumbers, but this is usually not regarded as a useful approach for calculating electronic transition shifts because of the larger change in helium solvation structure on electronic excitation. However, in the case of helium-tetracene, Fig. 1 shows that the difference potential ΔV is very small in the regions of strong helium binding, suggesting that the helium wavefunctions will be quite similar. We therefore expand the lowest energy helium wavefunction for the S_1 tetracene state about the corresponding helium wavefunction for the S_0 tetracene state, $|\Phi_0^1\rangle = |\Phi_0^0 + \Delta\Phi\rangle$. Evaluating the expectation value of $H_{S_1} = H + V_{S_1} = H_{S_0} + \Delta V$ in $|\Phi_0^1\rangle$ leads to the perturbative estimate for the spectral shift, $\Delta\nu = \langle\Phi_0^0|\Delta V|\Phi_0^0\rangle + \mathcal{O}(\Delta\Phi) = \langle\Delta V\rangle_{S_0} + \mathcal{O}(\Delta\Phi)$. Similarly, evaluating the expectation value of H_{S_0} in the helium state $|\Phi_0^0\rangle = |\Phi_0^1 + \Delta\Phi'\rangle$ leads to the alternative first order estimate $\Delta\nu = \langle\Delta V\rangle_{S_1} + \mathcal{O}(\Delta\Phi')$. Comparison of these two different first order estimates can provide a measure of the accuracy of the perturbative expansion.[31] The quantities $\langle\Delta V\rangle_{S_1}$ and $\langle\Delta V\rangle_{S_0}$ are readily calculated from VPI simulations using the S_1 and S_0 tetracene-helium interactions. Since the potential energy commutes with the position of the particles, and can thus be computed as a pure ground state quantity in VPI, for sufficiently long imaginary time paths this estimate of the shift can be made free of trial wavefunction bias. Additionally, this estimate takes advantage of correlated sampling: we use a single set of Markov chains to evaluate the potential energy difference [53] so that $\langle\Delta V\rangle_{S_1}$ and $\langle\Delta V\rangle_{S_0}$ are less subject to numerical noise than is the difference $E_{10} - E_{00}$.

3. Finite temperature shift

Calculating the spectral shift of the ZPL from PIMC calculations is complicated by the fact that multiple helium vibrational states may be populated at finite-temperature, i.e., $p_i \neq 0$ for several states $|\Phi_i\rangle$. While all states with nonzero population will be present in a finite-temperature calculation, weighted by their contribution to the thermal density matrix ρ, the average over ρ does not yield direct information about how different states contribute to a specific observable such as the position of the ZPL. Previously calculated frequencies of vibration for helium atoms on planar aromatic molecules indicate that thermal population of excited states at the simulation temperature of $T = 0.625$ K is unlikely [25, 26, 28, 36]. However, since we do not wish to explicitly exclude the possibility of thermal population of multiple He states here, we extend the above perturbative approach to define a shift for each He vibrational state, $\delta\nu_i \approx \langle \Delta V \rangle_{i,S_0}$, where the i subscript indicates that the expectation value is evaluated for the i^{th} He vibrational state. Evaluating the thermal average $\langle \Delta V \rangle_{S_0}$ in a finite temperature calculation using the interaction potential V_{S_0} then yields a thermal spectral shift $\sum_i p_i \Delta\nu_i$. Calculating also the thermal average $\langle \Delta V \rangle_{S_1}$ in addition will give some indication of how the finite-temperature vibrational ensemble in S_1 differs from that of S_0. By comparing the calculated values of $\langle \Delta V \rangle_{S_0}$ and $\langle \Delta V \rangle_{S_1}$ from the PIMC calculations of small clusters to values calculated from the VPI calculations for the same clusters, we can then assess whether there are significant contributions from thermally populated He states that are not present at $T = 0$.

III. RESULTS AND DISCUSSION

A. Helium configurations

Similar to what we have previously observed in studies of other PAMs in He clusters,[24, 25, 27] we find that the He density forms strongly localized layers close to the tetracene molecule. For all cluster sizes, we find that up to three helium atoms are strongly localized in positions along the long axis of the tetracene molecule (this constitutes the region between -1.0 Å $\leq y \leq 1.0$ Å in the first layer of He on each side of the molecule, see Fig. 1). Unlike the finite temperature situation for phthalocyanine, here only one helium configuration is found for each cluster in S_0 and S_1. The helium density profiles calculated from the finite-

temperature PIMC calculations are almost identical to those calculated from ground state VPI calculations. For economy of space, we therefore discuss below just the PIMC densities.

Constant z cuts of the helium density profiles from PIMC calculations for $N \leq 6$ are shown in Fig. 2. These cuts are taken at the location of the (equivalent) density maxima, and are oriented parallel to the xy plane. The tetracene molecule is also shown for reference, in skeletal bond form. The helium atoms in clusters with $N \leq 6$ are very strongly localized, with average energies of ~ -69.3 cm^{-1} and ~ -73.5 cm^{-1} per atom in the S_0 and S_1 states, respectively. Each helium atom is delocalized by ~ 3 Å along the molecular axis, consistent with the high zero-point energy in these small clusters. In contrast to previous models which assumed that the helium density is peaked above the global minima of the He-tetracene potential,[7] we find that the density is most strongly peaked above the two outer rings and directly over the central C-C bond of the tetracene molecule. This feature is due to the interplay of He-tetracene and He-He interactions and can be rationalized by reference to Fig. 3, which shows cuts of the He-tetracene potential along the $y = 0$ axis for two different values of z. Although the central location in the helium density corresponds with a potential barrier along the long axis of the molecule, the He-tetracene potential is still strongly attractive here and is only ~ 15 cm^{-1} smaller in magnitude than the global minima in the S_0 state (~ 10 cm^{-1} in the S_1 state.) However, placing the central atom at either of the two global minima would drive the outer atoms out of the locations above the outer wells due to He-He repulsion (~ 300 cm^{-1}), and is thus unfavorable energetically. Once these three sites are occupied, the helium-helium repulsions therefore drive additional atoms to outer regions of the He-tetracene potential energy surface. This trend is observed in calculations for both the S_0 and S_1 states of the molecule. As shown in Figures 1 and 3, the relative stabilization of the outer minima in the S_1 state and consequently also in the difference potential ΔV is larger in magnitude than that of the inner, global minima. Since the outer minima are first occupied at $N = 5, 6$, this explains why the spectral shift shows a rapid increase for these two cluster sizes, as was originally noted in the experimental study of Ref. 6.

These calculations show that, due to the interatomic repulsions of the helium atoms, the region of the helium-tetracene potential along the long axis of the molecule between -1.0 Å $y \leq 1.0$ Å (the region above the carbon skeleton, see Fig. 1), can support a maximum of three atoms. The equilibrium helium configuration for the next largest cluster $N = 8$

(Fig. 4) is, therefore, different than those found in the smaller clusters. We note here that both these PIMC densities and the VPI densities (not shown) for $N = 8$ contrast with those found in our previous ground state studies of He_8-tetracene (S_0) using the importance-sampled diffusion Monte Carlo (IS-DMC) method.[26] That earlier work indicated that four He atoms are strongly localized in the four minima along the long axis of the molecule (Fig. 1 of Ref. 26). In contrast, both the PIMC and VPI calculations show a structure having two atoms localized on each side of the molecule in the outer minima and two atoms localized along the y-axis, with the latter distributed over the saddle point separating the two global minima. Nevertheless, integrating the $N = 8$ density profile on one side of the molecule for all values of x, z and for -1.0 Å $\leq y \leq 1.0$ Å reveals that even in this cluster, for both S_0 and S_1 there are still only three He atoms located in the region above the carbon skeleton of tetracene, i.e., in the region of the four potential mimima. Both the VPI and PIMC calculations give lower average total and potential energies than the previous IS-DMC calculations: therefore it appears that the previous calculations did not converge to the true ground state. This was most likely due to inadequacies of the trial function, which is a common problem for strongly localized helium. The current study therefore nicely illustrates the utility of path integral methods in the study of systems where suitable trial functions are difficult to define due to the combined effects of a high degree of localization and high zero-point energy.

In clusters with $10 \leq N \leq 20$, we observe some N dependence of the equilibrium density profile, particularly in the S_0 state. The total number of He atoms located above and below the molecular plane, as determined from PIMC simulations, (i.e., not just the three atoms along the molecular axis) is listed in Table III for each cluster in this size regime. $N = 10$ is the only size with an even number of helium atoms for which there are unequal numbers of atoms on each side of the molecule. Figures 5-9 show the density profiles for structures having $M = 6 - 10$ atoms on one side of the tetracene molecule, for both the S_0 and S_1 electronic states of tetracene. These structures account for the helium configurations of all clusters with $10 \leq N \leq 20$. For example, the configuration for $N = 10$ has the density profile of $M = 4$ (Fig. 4) on one side of the molecule and that of $M = 6$ (Fig. 5) on the other side. These figures show that the helium density in the S_0 state is generally more highly delocalized than that in the S_1 state. This is consistent with the overall greater dispersive stabilization of the excited state (Fig. 1). In Fig. 9, we observe that for the largest number

of helium atoms, i.e., the configuration $M = 10$ on one side of the molecule that is found for the $N = 20$ cluster, the density in the S_0 state begins to more closely resemble that of the S_1 state. Thus as the packing density increases, the small differences between the two interaction potentials become less important.

In addition to these smaller clusters, we also studied clusters with $N = 24 - 150$. The density profiles for $N = 24$ and $N = 96$ are shown in Figures 10 and 11. In all of these larger clusters, for both S_0 and S_1 states of tetracene we find a single equilibrium configuration of helium atoms close to the tetracene molecule in which three He atoms are strongly localized on each side of the molecule. In agreement with our previous studies of the benzene molecule, [24] we find that these strongly localized atoms are only weakly coupled to other atoms in the first solvation shell by permutations. The lack of any significant N dependence of the density profile indicates that for $N \geq 24$ the presence of additional helium atoms suppresses the variability of configurations that was found in the S_0 calculations for the smaller clusters with $10 \leq N \leq 20$. This is likely due to greater packing of helium atoms into the most attractive regions of the He-tetracene potential for these larger clusters. The resulting strong He-He repulsions lead to more strongly localized configurations than are seen in the smaller clusters. In order to investigate how the helium density differs in the S_0 and S_1 states for the clusters with $N \geq 10$, we examine the difference density $\Delta\rho = \rho_{S_0} - \rho_{S_1}$. This is shown for $N = 16$, 48, and 96 in Fig. 12. It is evident that the primary differences between S_0 and S_1 densities are a more diffuse central peak along the x axis in the S_0 state, with the outer peaks consequently shifted slightly further outward due to He-He repulsions. This difference in the densities can be understood simply by examining a cut of the He-tetracene potentials along $y = 0$ (Fig. 3); the lowering of the central barrier height relative to the potential minima in the S_1 state accounts for the concentration of helium density closer to the origin. While the general character of the differences in the densities in S_0 and S_1 is similar for all clusters with $N \geq 10$, the magnitude of the differences in the clusters with $N \geq 24$ is greatly reduced compared to the differences in the smaller clusters, as is shown in Fig. 12, due to the greater degree of localization of He atoms in the larger clusters.

B. Spectral shift

The spectral shift of the $S_0 \rightarrow S_1$ transition of tetracene relative to the gas phase absorption frequency calculated from both ground state VPI and finite temperature PIMC simulations according to the three approaches described above is shown in Fig. 13 as a function of N for ^4He_N-tetracene clusters with $N \leq 20$, the small cluster size regime for which experimental data exist. The triangles represent the experimentally measured spectral shift from Ref. 6. The spectral shift is seen to increase approximately linearly with N for $N \leq 4$. At $N = 5, 6$ there is a rapid increase in the magnitude of the shift, which then continues to increase at a slower rate for larger cluster sizes. Examining Fig. 13, it is apparent that the semi-empirical S_1 interaction potential yields calculated values of the spectral shift that are in excellent agreement with experimental data for clusters with $N \leq 5$. In clusters with $N = 6, 8$ the calculated spectral shift differs from the experimentally measured values by $\sim 6 - 7$ cm^{-1}. In spite of these small discrepancies, the overall trends in the experimental data and the calculated values are very similar and in good agreement. For $N \leq 8$ we find good agreement between the spectral shifts calculated from the ground state He energies in S_0 and S_1 (approach 1) and both the $T = 0$ (approach 2) and $T = 0.625$ K (approach 3) values of the perturbative estimates of the shift. For larger clusters the perturbative estimates in a given electronic state also do not show a strong temperature dependence. We therefore conclude that, at $T = 0.625$ K, the He atoms are primarily in the many-body ground state. However, for $N \geq 10$ the two perturbative estimates $\langle \Delta V \rangle_{S_0}$ and $\langle \Delta V \rangle_{S_1}$ show a systematic difference. Noting that the calculated value of the spectral shift can be quite sensitive to the configuration of atoms in a cluster, as reported previously in studies of anthracene[36] and phthalocyanine, [27] we attribute this to the differences in the He many-body states for the two electronic states that are reflected in the observed differences in the He density profiles (Figs. 5 - 10).

For clusters with $N \geq 10$, all three approaches for calculation of the spectral shift yield values that are consistently smaller in magnitude than the experimental values (Fig. 13) by ~ 10 cm^{-1}. There are at least two possible reasons for this. One is that the difference may reflect inaccuracies in both the S_0 and S_1 interaction potentials. While it may be possible to improve the agreement between the simulations and the experimental values by re-parametrizing the S_1 interaction potential for larger clusters, this was not pursued here

due to the approximate nature of both S_0 and S_1 potential energy representations. It is also possible that the first order error $\mathcal{O}(\Delta\Phi_0)$ is larger for the perturbative estimate using the S_0 potential energy surface than the S_1 surface. Deeper investigation of this issue would require the use of a sophisticated electronic structure method with the ability to accurately treat non-local, dispersive interactions very accurately in both the ground and excited molecular states. Another possible source of discrepancy between the theoretical values calculated here and the experimentally measured ones could stem from differences in how clusters are formed experimentally and how they are simulated here. The spectral shift data of Ref. 6 are obtained from absorption measurements. If the helium density configuration does not change upon absorption of light, the spectral shift measured in the absorption experiment should correspond to the spectral shift due to the equilibrium configuration in the S_0 state. In contrast, our calculations indicate that the calculated spectral shift from the S_1 state agrees more closely with the experimental data for $10 \leq N \leq 20$, as shown in Fig. 13. This might indicate that the configurations of helium that are achieved in the experiment more closely resemble those calculated for the S_1 electronic state. The experimental measurements of Even *et al.* were accomplished using a method by which the tetracene molecules are cooled to ~ 0.4 K prior to the formation of the clusters.[6] Once the molecule is cool, the clusters are formed in a step-wise fashion via collisions of the molecule with the helium carrier gas.[54] During this process, it is possible that the helium clusters form in a manner consistent with what we observe for the smallest clusters studied here, with six atoms first preferentially filling the 3 sites on each side of the molecule. If the clusters are not thermalized during the time scale of the experiment, then structures other than the helium ground state of S_0, and which are more similar to the helium configurations in S_1, may be formed. Our simulation method places N atoms at random positions in the simulation cell, then determines the equilibrium distribution of helium based on the thermal density matrix for the system Hamiltonian. Developing a better understanding of the cluster formation process would require a real time quantum dynamical simulation method beyond the capabilities of this study.

Spectral shift data for the larger clusters are shown in Figure 14. For the larger clusters, we find that the magnitude of the shift increases smoothly and monotonically as N increases. The difference between $\langle \Delta V \rangle_{S_0}$ and $\langle \Delta V \rangle_{S_1}$ is relatively constant at a value of $\sim 3-4$ cm^{-1} for clusters with $N \geq 20$, indicating that the differences in the helium configurations for the

two electronic states of the molecule are likely located within the layers of helium that are most strongly localized close to the molecular surface.

In typical He droplet experiments, there are $\sim 10^4$ He atoms in a droplet. In order to make a comparison of our results with the experimentally measured spectral shift for tetracene in a He droplet, we fit our data for $N \geq 20$ from both the S_0 and S_1 perturbative estimates to exponential functions of the form $\Delta\nu(N) = ae^{-b/N}$ and then evaluate this for $N = 10^4$. Given the first order origin of the two perturbative estimates, it is reasonable to expect that the actual large droplet value will lie between the two extrapolated values. This results in an estimated bound for the spectral shift $\Delta\nu$ as lying between -93.6 and -90.7 cm^{-1}, which is approximately 90 % of the experimentally measured droplet value of -103.1 cm^{-1}.[5] We take this as good agreement, given the semi-empirical nature of the excited state interaction potential employed here.

IV. SUMMARY AND CONCLUSIONS

We have utilized the path integral Monte Carlo method to calculate the spectral shift and analyze the configurations of helium in He$_N$-tetracene clusters with N ranging from 1 to 150. The calculated values of the spectral shift are in good agreement with the experimental findings of Even *et al.* [6] for the smallest clusters studied. For intermediate size clusters with $10 \leq N \leq 20$, we find a weak systematic discrepancy from the experimental results, with the theoretical estimates yielding somewhat smaller values of the shift. This difference is attributed to either possible inadequacies of the helium-tetracene potentials or possible non-equilibrium effects in the formation of helium configurations in the small cluster experiment [6], or to a combination of both.

In this study, we find that while there is some N dependence of the helium configurations in small clusters with $10 \leq N \leq 20$ in the S_0 state, there is no evidence for multiple configurations in any clusters. The largest clusters, for which the first solvation shell is complete or nearly complete (this happens at between 24 and 48 He atoms), should provide the closest analogy to the large droplet ($N \sim 10^4$) experimental studies of tetracene in helium. Our results suggest that, in contrast to the emission spectral splitting of phthalocyanine [15, 27], the zero-phonon line splitting of tetracene in helium droplets is not due to different static metastable configurations of helium close to the molecule. This is further supported by the

experimentally observed lack of interconversion between the α and α' states in the S_1 state in large helium droplets,[12, 14] which is in strong contrast to what was observed in the corresponding pump-probe spectra of phthalocyanine.[16] We note that after the present study was completed, an experimental study of biphenylene in helium droplets appeared in which zero phonon line splitting was also observed.[21] In that work it was concluded on the basis of inspection of the helium-molecule interaction potential that a splitting origin deriving from multiple metastable configurations was unlikely.

The present quantum Monte Carlo results also suggest that the multiple configurations that were observed for phthalocyanine in Ref. 27 and noted there to be related to the commensurate-incommensurate transition observed for helium atoms adsorbed on graphite [55], are a characteristic of a 2D adsorbing surface and will in general not present for linear, predominantly 1D adsorbing systems such as tetracene. We therefore conclude that the ZPL splitting of the absorption and emission spectra of tetracene in helium droplets is likely due to a dynamic characteristic of the adsorbed helium atoms rather than to a static structural characteristic. This will be addressed in a forthcoming publication.[30]

V. ACKNOWLEDGMENTS

We are grateful to Prof. J. P. Toennies for discussions which inspired us to pursue this project and to A. Slenzcka and R. Lehnig for discussion of their experimental data. H. D. Whitley acknowledges the support of the AFOSR through an NDSEG research fellowship. This work performed, in part, under the auspices of the U.S. Department of Energy by Lawrence Livermore National Laboratory under Contract DE-AC52-07NA27344.

---

[1] See the articles under the Special Topic *Helium nanodroplets: a novel medium for chemistry and physics*, edited by R. E. Miller and K. B. Whaley, in J. Chem. Phys. **115**, 10065–10281 (2001).

[2] F. Stienkemeier and A. F. Vilesov, J. Chem. Phys. **115**, 10119 (2001).

[3] F. Steinkemeier and K. K. Lehmann, J. Phys. B: At. Mol. Opt. Phys. **39**, R127 (2006).

[4] F. Paesani, Y. Kwon, and K. B. Whaley, Phys. Rev. Lett. **94**, 114306 (2005).

[5] M. Hartmann, A. Lindinger, J. P. Toennies, and A. F. Vilesov, Chem. Phys. **239**, 139 (1998).

[6] U. Even, I. Al-Hroub, and J. Jortner, J. Chem. Phys. **115**, 2069 (2001).

[7] M. Hartmann, A. Lindinger, J. P. Toennies, and A. F. Vilesov, J. Phys. Chem. A **105**, 6369 (2001).

[8] A. Lindinger, J. P. Toennies, and A. F. Vilesov, Phys. Chem. Chem. Phys. **3**, 2581 (2001).

[9] N. Pörtner, A. F. Vilesov, and M. Havenith, Chem. Phys. Lett. **343**, 281 (2001).

[10] M. Hartmann, A. Lindinger, J. P. Toennies, and A. F. Vilesov, Phys. Chem. Chem. Phys. **4**, 4839 (2002).

[11] A. Lindinger, J. P. Toennies, and A. F. Vilesov, J. Chem. Phys. **121**, 12282 (2004).

[12] R. Lehnig and A. Slenczka, J. Chem. Phys. **122**, 244317 (2005).

[13] A. Lindinger, J. P. Toennies, and A. F. Vilesov, Chem. Phys. Lett. **429**, 1 (2006).

[14] A. Lindinger, E. Lugovoj, J. P. Toennies, and A. F. Vilesov, Z. Phys. Chem. **215**, 401 (2001).

[15] R. Lehnig and A. Slenczka, J. Chem. Phys. **118**, 8256 (2003).

[16] R. Lehnig and A. Slenczka, J. Chem. Phys. **120**, 5064 (2004).

[17] R. Lehnig and A. Slenczka, Chem. Phys. Chem. **5**, 1014 (2004).

[18] R. Schmied, P. Carcabal, A. M. Doktor, V. P. A. Lonij, K. K. Lehmann, and G. Scoles, J. Chem. Phys. **121**, 2701 (2004).

[19] R. Lehnig, M. Slipchenko, S. Kuma, T. Momose, B. Saratakov, and A. Vilesov, J. Chem. Phys. **121**, 9396 (2004).

[20] R. Lehnig, J. A. Sebree, and A. Slenczka, J. Phys. Chem. A **111**, 7576 (2007).

[21] O. Birer, P. Moreschini, K. K. Lehmann, and G. Scoles, J. Phys. Chem. A **111**, 7624 (2007).

[22] S. Kuma, H. Goto, M. N. Slipchenko, A. F. Vilesov, A. Khramov, and T. Momose, J. Chem. Phys. **127**, 214301 (2007).

[23] O. Birer, P. Moreschini, and K. K. Lehmann, Phys. Chem. Chem. Phys. **10**, 1648 (2008).

[24] Y. Kwon and K. B. Whaley, J. Chem. Phys. **114**, 3163 (2001).

[25] P. Huang and K. B. Whaley, Phys. Rev. B **67**, 155419 (2003).

[26] P. Huang, H. D. Whitley, and K. B. Whaley, J. Low Temp. Phys. **134**, 263 (2004).

[27] H. D. Whitley, P. Huang, Y. Kwon, and K. B. Whaley, J. Chem. Phys. **123**, 054307 (2005).

[28] M. Xu and Z. Bačić, J. Phys. Chem. A **111**, 7653 (2007).

[29] B. R. Gibbons, M. Xu, and Z. Bačić, J. Phys. Chem. A **113**, 3789 (2009).

[30] H. D. Whitley, J. L. DuBois, and K. B. Whaley (2009), in preparation.

[31] D. Blume, M. Lewerenz, F. Huisken, and M. Kaloudis, J. Chem. Phys. **105**, 8666 (1996).

[32] R. A. Aziz, F. R. W. McCourt, and C. C. K. Wong, Mol. Phys. **61**, 1487 (1987).

[33] W. E. Carlos and M. W. Cole, Surf. Sci. **91**, 339 (1980).

[34] V. L. Ginzburg and A. A. Sobaynin, Sov. Phys. Usp. **19**, 773 (1976).

[35] E. Shalev, N. Ben-Horin, U. Even, and J. Jortner, J. Chem. Phys. **95**, 3147 (1991).

[36] A. Heidenreich, U. Even, and J. Jortner, J. Chem. Phys. **115**, 10175 (2001).

[37] A. Heidenreich and J. Jortner, J. Chem. Phys. **118**, 10101 (2003).

[38] We follow the IUPAC numbering convention for planar aromatic hydrocarbons, see, for example, F. A. Carey, *Organic Chemistry* (The McGraw-Hill Companies, New York, 1996).

[39] A. Sarsa, K. E. Schmidt, and W. Margo, J. Chem. Phys. **113**, 1366 (2000).

[40] J. E. Cuervo, P.-N. Roy, and M. Boninsegni, J. Chem. Phys. **122**, 114504 (2005).

[41] P. Huang, Ph.D. thesis, University of California, Berkeley (2003).

[42] D. M. Ceperley, Rev. Mod. Phys. **67**, 279 (1995).

[43] S. A. Chin, Phys. Lett. A **226**, 344 (1997).

[44] M. H. Kalos and P. A. Whitlock, *Monte Carlo Methods*, vol. 1 (John Wiley & Sons, Inc., New York, 1986).

[45] B. L. Hammond, W. A. Lester, Jr., and P. J. Reynolds, *Monte Carlo Methods in Ab Initio Quantum Chemistry* (World Scientific, Singapore, 1994).

[46] E. L. Pollock and D. M. Ceperley, Phys. Rev. B **30**, 2555 (1984).

[47] P. Huang, Y. Kwon, and K. B. Whaley, in *Quantum Fluids in Confinement*, edited by E. Krotscheck and J. Navarro (World Scientific, Singapore, 2002), vol. 4 of *Advances in Quantum Many-Body Theories*, p. 91, physics/0204089.

[48] R. Zillich, F. Paesani, Y. Kwon, and K. B. Whaley, J. Chem. Phys. **123**, 114306 (2005).

[49] G. C. Schatz and M. A. Ratner, *Quantum Mechanics in Chemistry* (Prentice Hall, Englewood Cliffs, NJ, 1993).

[50] M. Hartmann, R. E. Miller, J. P. Toennies, and A. Vilesov, Phys. Rev. Lett. **75**, 1566 (1995).

[51] F. Paesani, F. A. Gianturco, and K. B. Whaley, J. Chem. Phys. **115**, 10225 (2001).

[52] H. Li, N. Blinov, P.-N. Roy, and R. J. L. Roy, J. Chem. Phys. **130**, 144305 (2009).

[53] Y. Kwon and K. B. Whaley, J. Chem. Phys. **115**, 10146 (2001).

[54] U. Even, J. Jortner, D. Noy, and N. Lavie, J. Chem. Phys. **112**, 8068 (2000).

[55] D. M. Ceperley and E. Manousakis, J. Chem. Phys. **115**, 10111 (2001).

[56] C. A. Coulson and P. L. Davies, Trans. Faraday Soc. **48**, 777 (1952).

[57] A. Steiweiser, *Molecular Orbital Theory for Organic Chemists* (Wiley, New York, 1961).

[58] *CRC Handbook of Chemistry and Physics* (CRC, Boca Raton, FL, 1981), 62nd ed.

TABLE I: Interaction potential parameters for helium with tetracene.

Pair	σ/Å	ϵ/(K)
He-C	2.74	16.3
He-H	3.21	6.00

TABLE II: Parameters for the S_1 interaction potential.

Huckel parameters[56, 57]		
Pair	Resonance integral (eV)	Coulomb integral (eV)
C-C	-1.70	0
Other parameters[36, 58]		
α	0.204 Å	
$\bar{F}$	24.5 eV	
η	0.4	
σ_{ex}/σ	1.0298	

TABLE III: Configurations (above|below) for clusters with $10 \leq N \leq 20$.

N	S_0	S_1
8	(4|4)	(4|4)
10	(4|6)	(4|6)
12	(6|6)	(6|6)
14	(7|7)	(7|7)
16	(8|8)	(8|8)
17	(8|9)	(9|8)
18	(9|9)	(9|9)
20	(10|10)	(10|10)

FIG. 1. The (a) S_0 and (b) S_1 helium-tetracene interaction potential in wavenumbers near the global minimum at $z = 2.69$ Å. The skeletal bond form of the tetracene molecule is also shown for reference. Contours are shown from the global minima up to about 40 cm^{-1}. The surface of the carbon skeleton of the tetracene molecule is restricted to the region -1.0 Å $\leq y \leq 1.0$ Å and -5.0 Å $\leq x \leq 5.0$ Å. (c) The difference in the S_0 and S_1 helium-tetracene interaction potentials, $V_{S_1} - V_{S_0}$, shown in wavenumbers, near the global minimum at $z = 2.69$ Å. The overall difference is repulsive near the carbons in the 9, 10, 11, and 12 positions (using the numbering systems of Ref. 38), due to the inclusion of ΔV_{LJ}. Contours are shown only for $V_{S_1} - V_{S_0} \leq 2.0$ cm^{-1}.

FIG. 2. Parallel cuts of the helium densities seen in $N = 1 - 6$ clusters at the maxima ($z \approx \pm 2.7$ Å) in the S_0 (left) and S_1 (right) states, calculated via PIMC simulations at $T = 0.625$ K. The top panel shows one He atom localized at the molecule (seen for $N = 1, 2, 3$), the center panel shows two atoms at the molecule (seen for $N = 3, 4, 5$), while the lower panel shows three atoms localized near the molecule (seen for $N = 5, 6$).

FIG. 3. Cuts of the He-tetracene potentials along $y = 0$ near the global minima for the S_0 and S_1 states.

FIG. 4. Cuts of the helium densities for $N = 8$ atoms near tetracene at the density maxima ($z \approx \pm 2.8$ Å) in the S_0 (left) and S_1 (right) electronic states of tetracene, calculated via PIMC simulations at $T = 0.625$ K. Contours are shown in the density range $0.05 \leq \rho \leq 1.0$.

FIG. 5. Density profile for $M = 6$ He atoms on one side of the tetracene molecule, calculated via PIMC simulations at $T = 0.625$ K. Profiles in the left (right) panels correspond to the S_0 (S_1) state. Contours are shown for two planes parallel to the molecule at $z \approx 3.6$ Å in the upper panels and at $z \approx 2.9$ Å in the lower panels. The cuts shown are taken from a single PIMC simulation and do not necessarily reflect the full symmetry of the cluster that would result from averaging over many runs.

FIG. 6. Density profile for $M = 7$ He atoms on one side of the tetracene molecule,

calculated via PIMC simulations at $T = 0.625$ K. Profiles in the left (right) panels correspond to the S_0 (S_1) state. Contours are shown for two planes parallel to the molecule at $z \approx 3.6$ Å in the upper panels and at $z \approx 3.0$ Å in the lower panels. The cuts shown are taken from a single PIMC simulation and do not necessarily reflect the full symmetry of the cluster that would result from averaging over many runs .

FIG. 7. Density profile for $M = 8$ He atoms on one side of the tetracene molecule, calculated via PIMC simulations at $T = 0.625$ K. Profiles in the left (right) panels correspond to the S_0 (S_1) state. Contours are shown for two planes parallel to the molecule at $z \approx 3.6$ Å in the upper panels and at $z \approx 3.0$ Å in the lower panels. The cuts shown are taken from a single PIMC simulation and do not necessarily reflect the full symmetry of the cluster that would result from averaging over many runs.

FIG. 8. Density profile for $M = 9$ He atoms on one side of the tetracene molecule, calculated via PIMC simulations at $T = 0.625$ K. Profiles in the left (right) panels correspond to the S_0 (S_1) state. Contours are shown for two planes parallel to the molecule at $z \approx 3.6$ Å in the upper panels and at $z \approx 3.0$ Å in the lower panels. The cuts shown are taken from a single PIMC simulation and do not necessarily reflect the full symmetry of the cluster that would result from averaging over many runs.

FIG. 9. Density profile for $M = 10$ He atoms on one side of the tetracene molecule. Profiles in the left (right) panels correspond to the S_0 (S_1) state. Contours are shown for two planes parallel to the molecule at $z \approx 3.6$ Å in the upper panels and at $z \approx 2.9$ Å in the lower panels. The cuts shown are taken from a single PIMC simulation and do not necessarily reflect the full symmetry of the cluster that would result from averaging over many runs.

FIG 12. The integrated difference in the helium density profiles for the first layer of He near tetracene in the S_0 (ρ_{S_0}) and S_1 (ρ_{S_1}) for clusters with $N = 16$, $N = 48$, and $N = 96$ helium atoms, calculated via PIMC simulations at $T = 0.625$ K. For $N = 48$ and $N = 96$ the difference has been integrated for -4.0 Å $\leq z \leq 4.0$ Å so that only the first layer of helium near the molecule is considered. The plots shown are derived from a single

PIMC simulation in each electronic state and do not necessarily reflect the full symmetry of the cluster that would result from averaging over many runs.

FIG. 10. Cuts of the helium density profile at the maximum density for $N = 24$ at $z \approx 2.8$ Å (upper panels) and $z \approx -2.8$ Å (lower panels), , calculated via PIMC simulations at $T = 0.625$ K. The left panels show results from calculations in the S_0 electronic state of tetracene. Results from calculations in the S_1 state are shown in the panel on the right.

FIG. 11. Cuts of the helium density profile at the maximum density for $N = 96$ at $z \approx 2.8$ Å (upper panels) and $z \approx -2.8$ Å (lower panels), calculated via PIMC simulations at $T = 0.625$ K. The left panels show results from calculations in the S_0 electronic state of tetracene. Results from calculations in the S_1 state are shown in the panel on the right.

FIG. 13. Spectral shift of the tetracene $S_0 \rightarrow S_1$ transition as a function of the number of helium atoms in a He cluster with $N \leq 20$. Experimental data (triangles) are taken from Ref. 6. The inset shows the same data in the region of $1 \leq N \leq 4$. The standard deviations of the plotted data are all ≤ 0.05 cm^{-1}, and are much smaller than the symbols shown on the plots. The experimentally measured point for $N = 20$ has been shown with an error bar of ± 3 cm^{-1} since this value was not reported with certainty.

FIG. 14. Spectral shift of the tetracene $S_0 \rightarrow S_1$ transition as a function of the number of helium atoms in a He cluster from PIMC simulations at $T = 0.625$ K. Data for $N \geq 20$ are fit by an exponential function, $\Delta\nu(N) = ae^{-b/N}$ (dotted lines). Standard deviations of the pertubatively calculated spectral shift for $N \geq 20$ are ≤ 0.10 cm^{-1}.

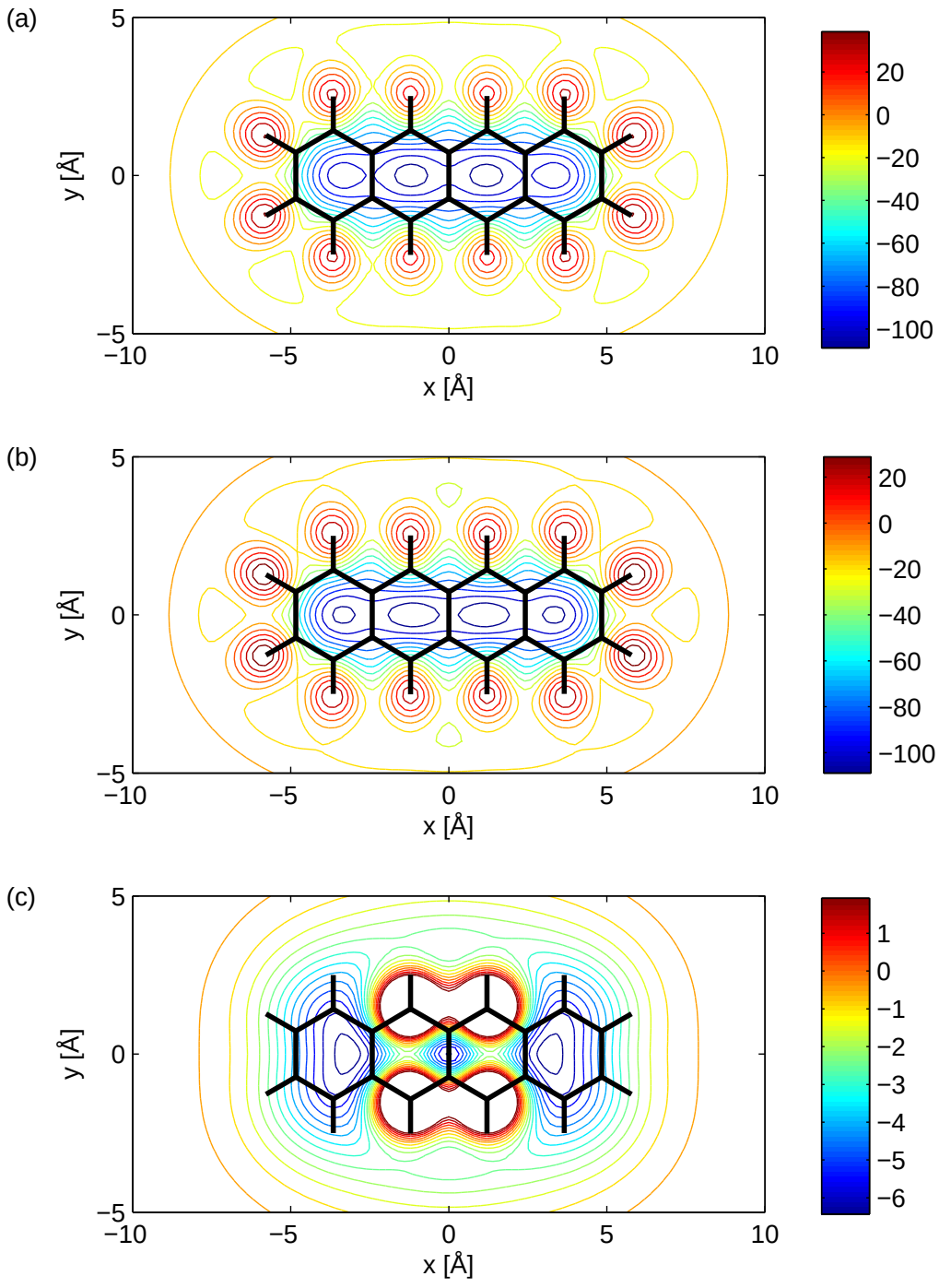

FIG. 1: Whitley *et al.* *The Journal of Chemical Physics*

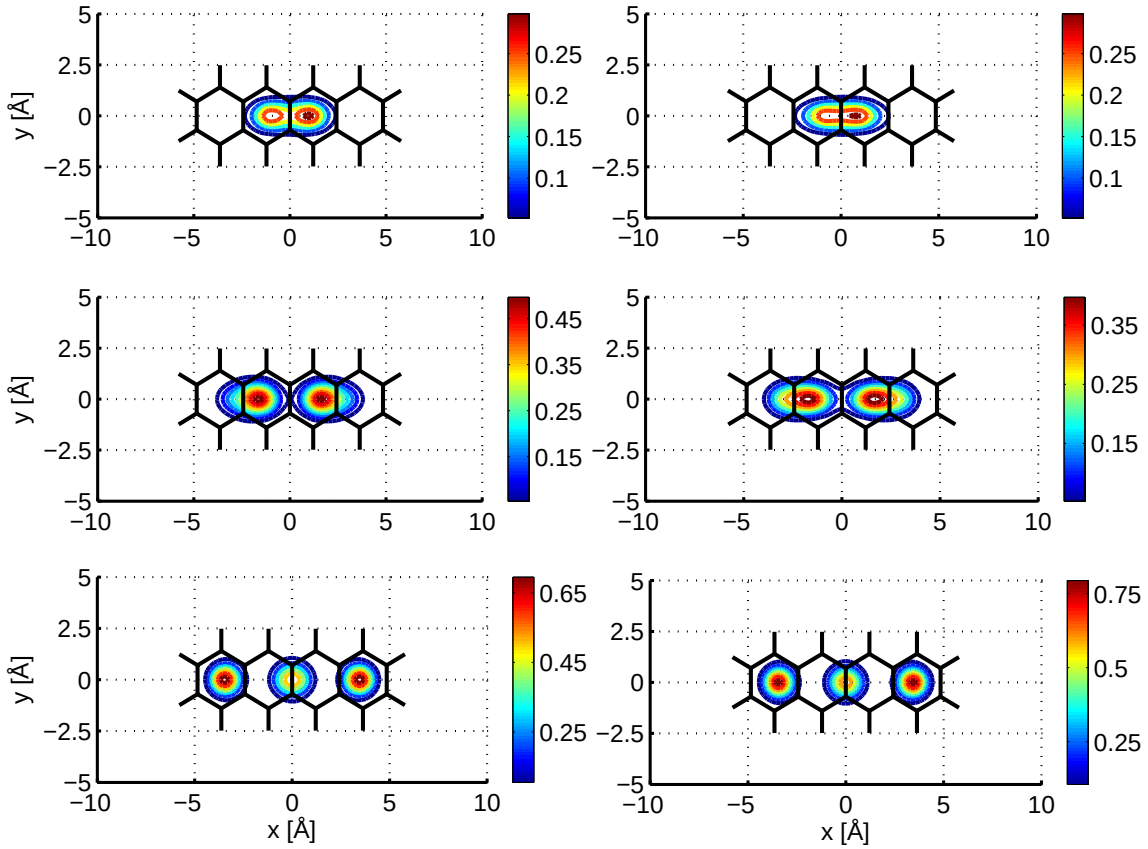

FIG. 2: Whitley *et al.* *The Journal of Chemical Physics*

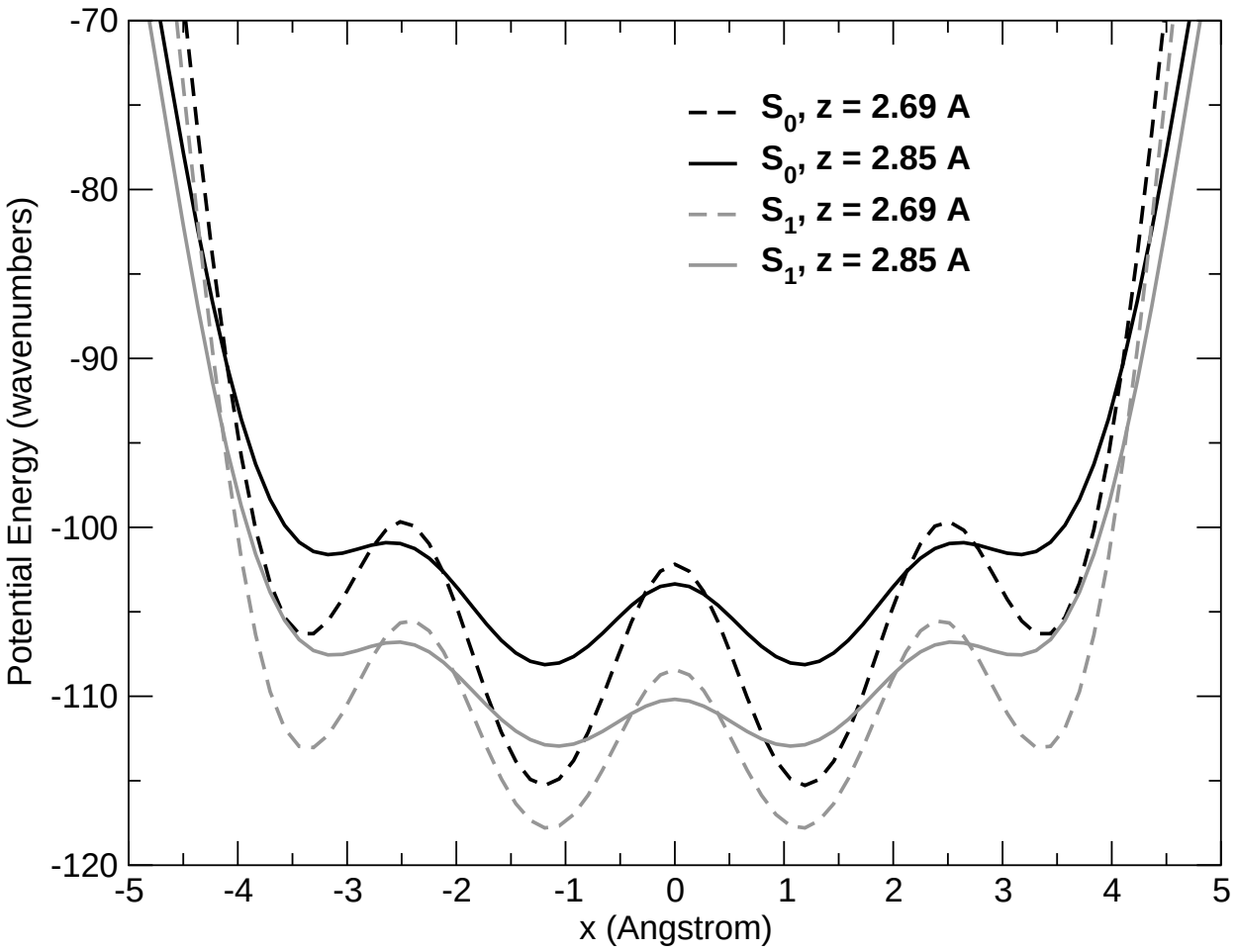

FIG. 3: Whitley *et al.* *The Journal of Chemical Physics*

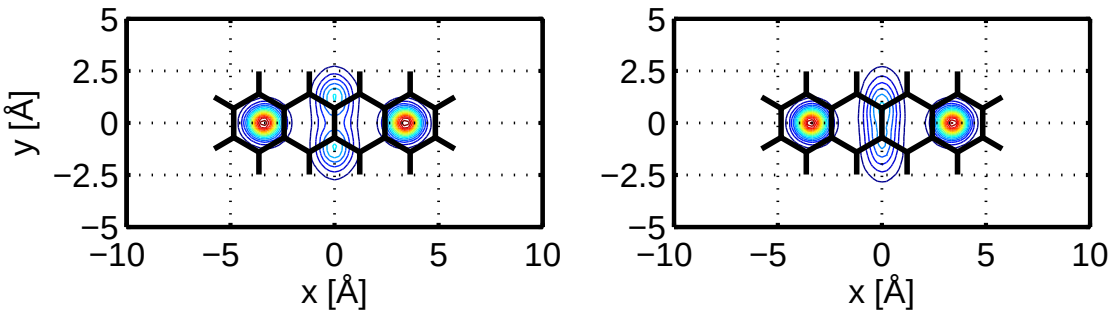

FIG. 4: Whitley *et al.* *The Journal of Chemical Physics*

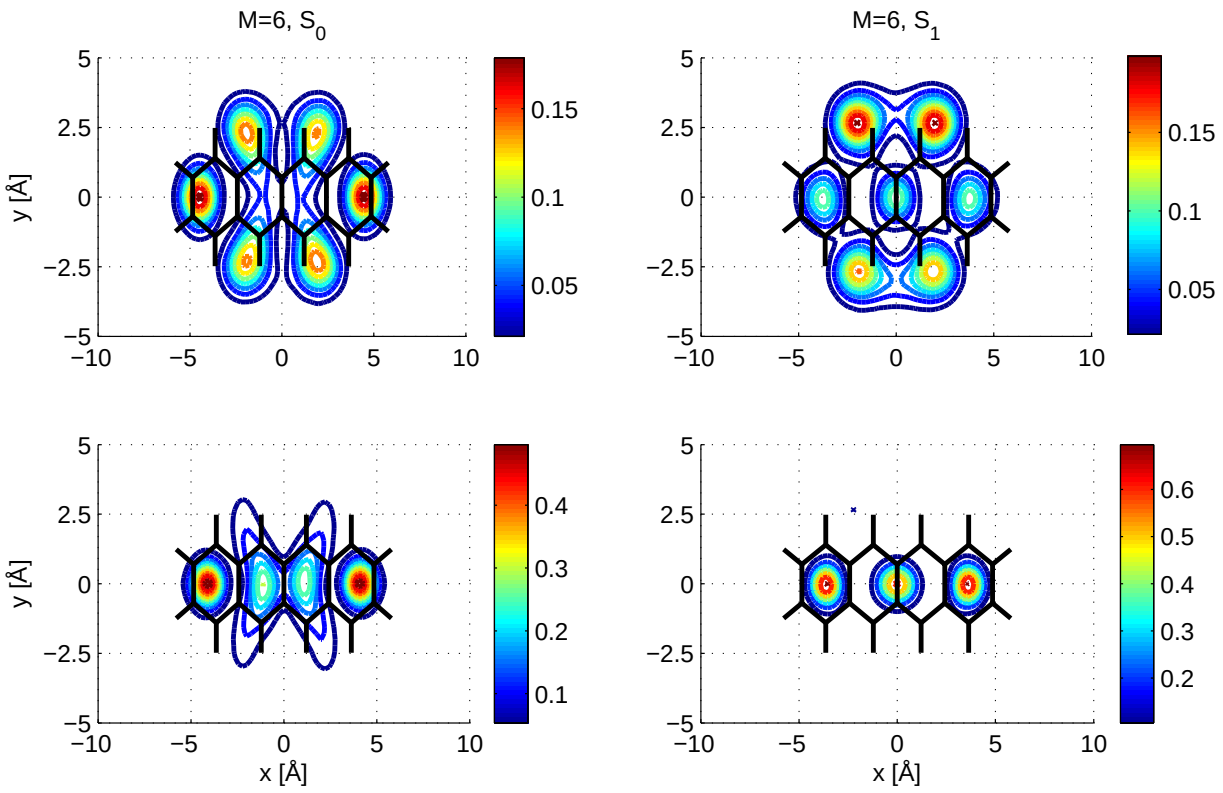

FIG. 5: Whitley *et al.* *The Journal of Chemical Physics*

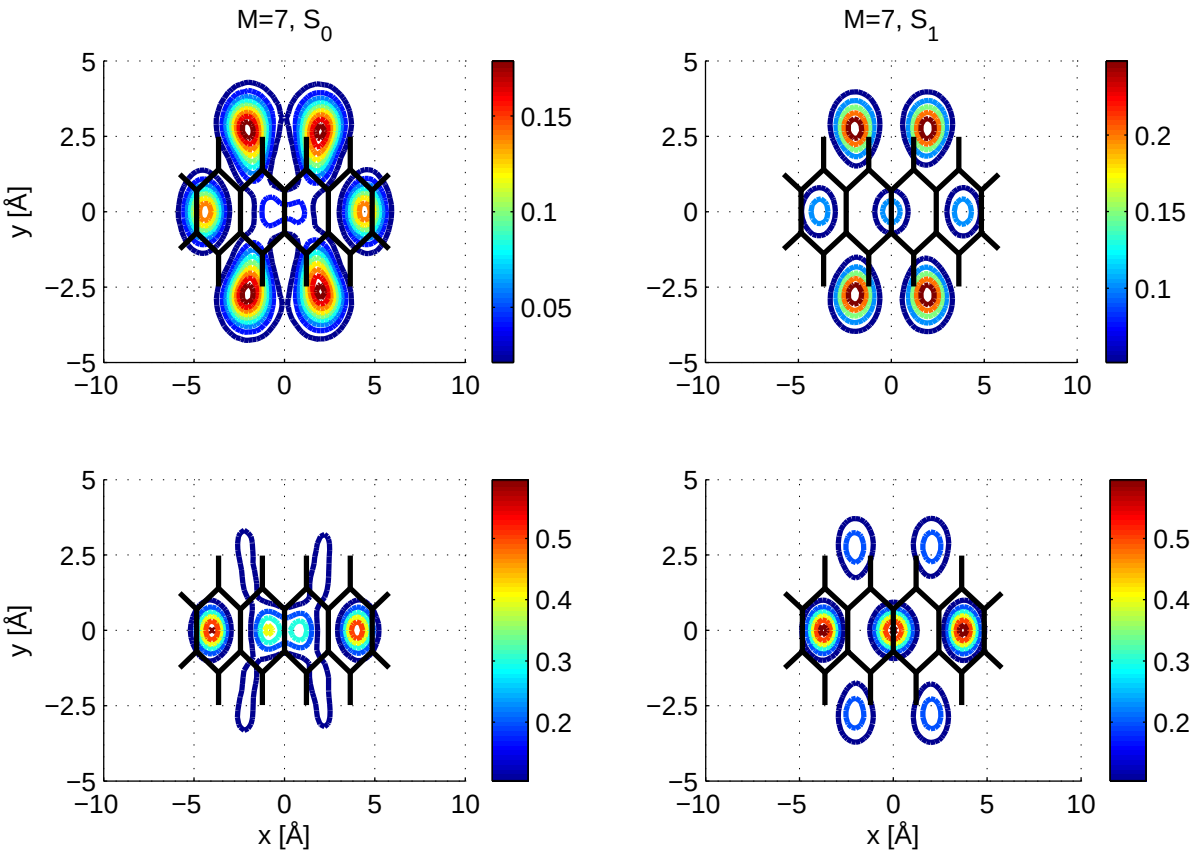

FIG. 6: Whitley *et al.* *The Journal of Chemical Physics*

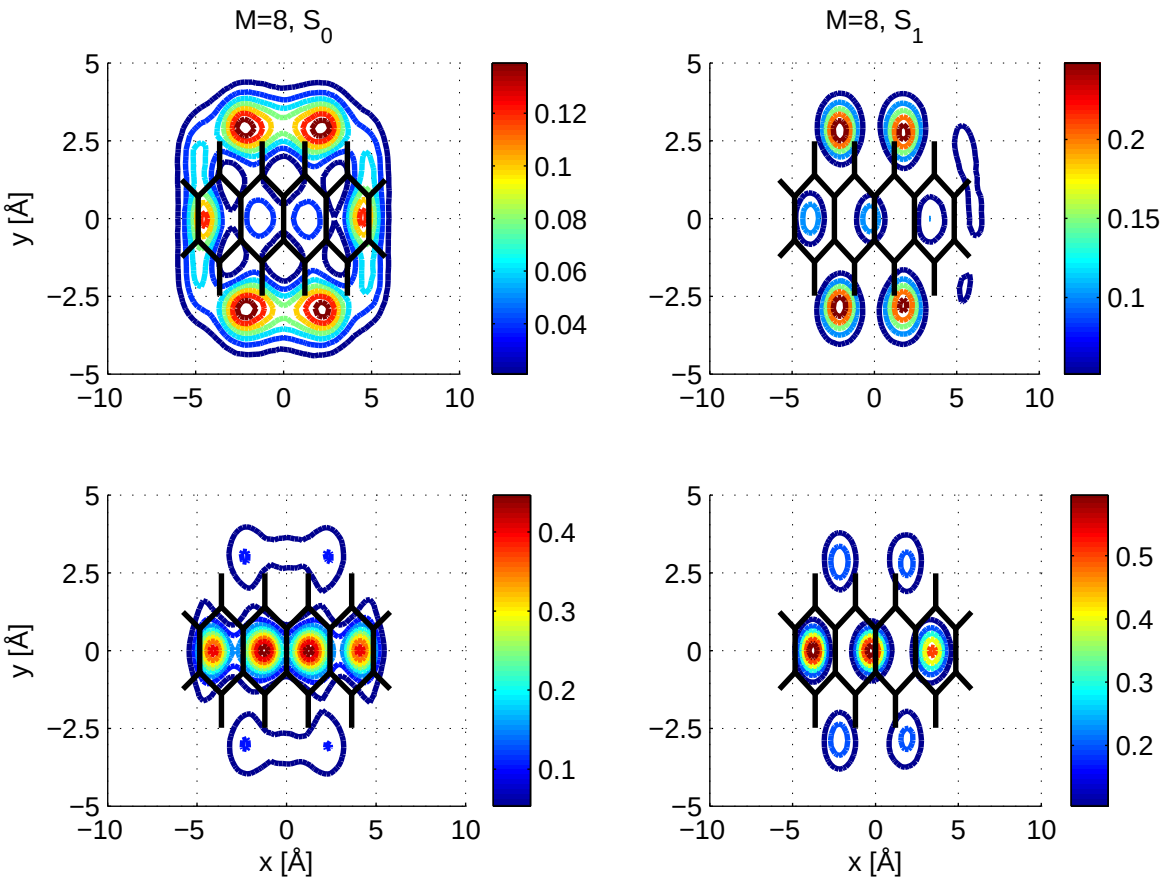

FIG. 7: Whitley *et al.* *The Journal of Chemical Physics*

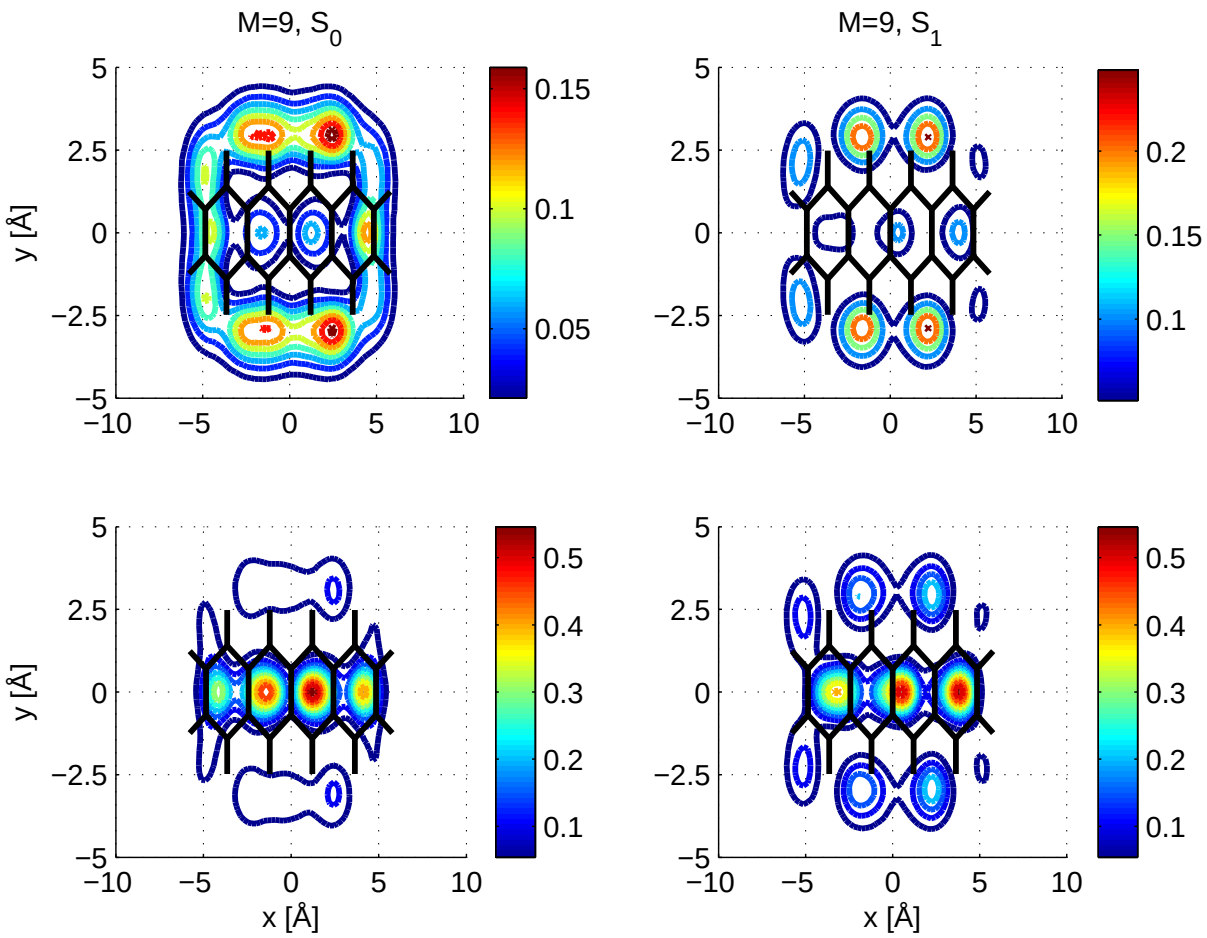

FIG. 8: Whitley *et al.* *The Journal of Chemical Physics*

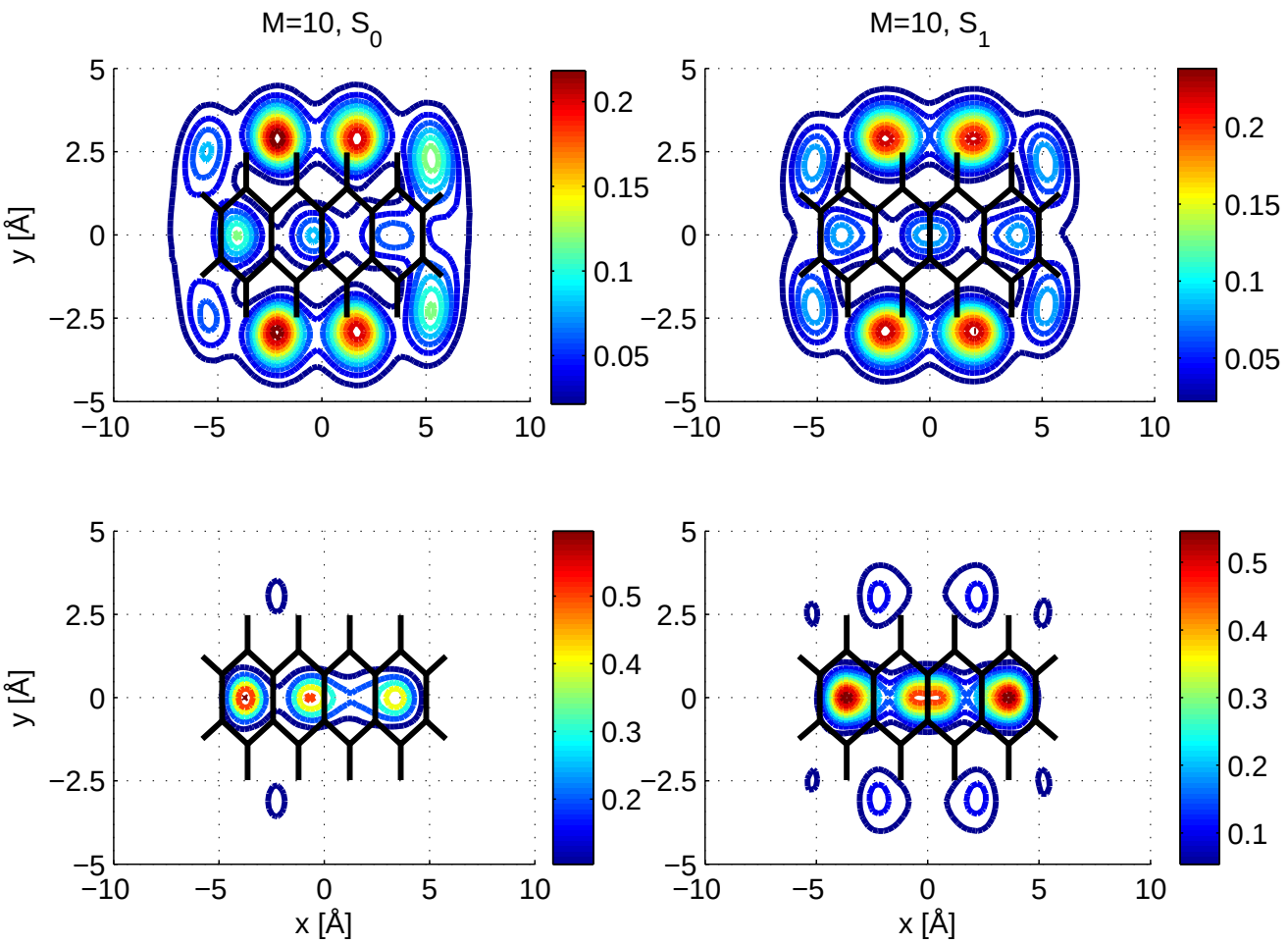

FIG. 9: Whitley *et al.* *The Journal of Chemical Physics*

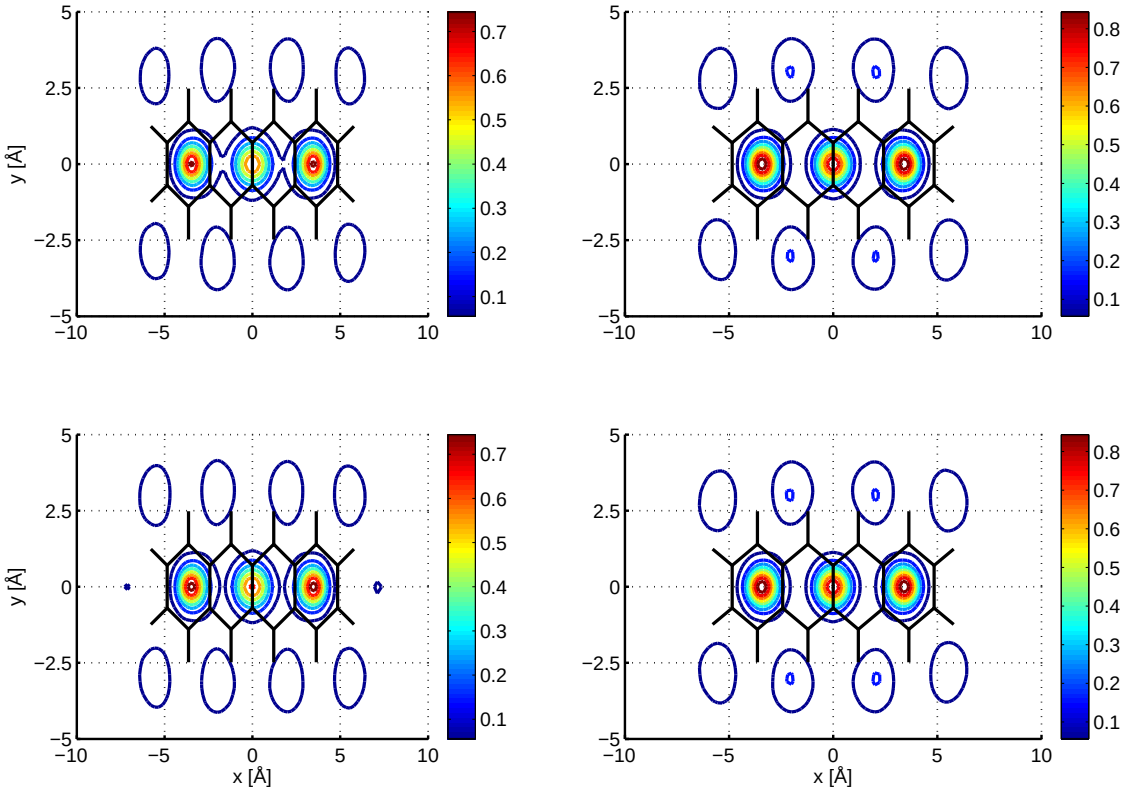

FIG. 10: Whitley *et al.* *The Journal of Chemical Physics*

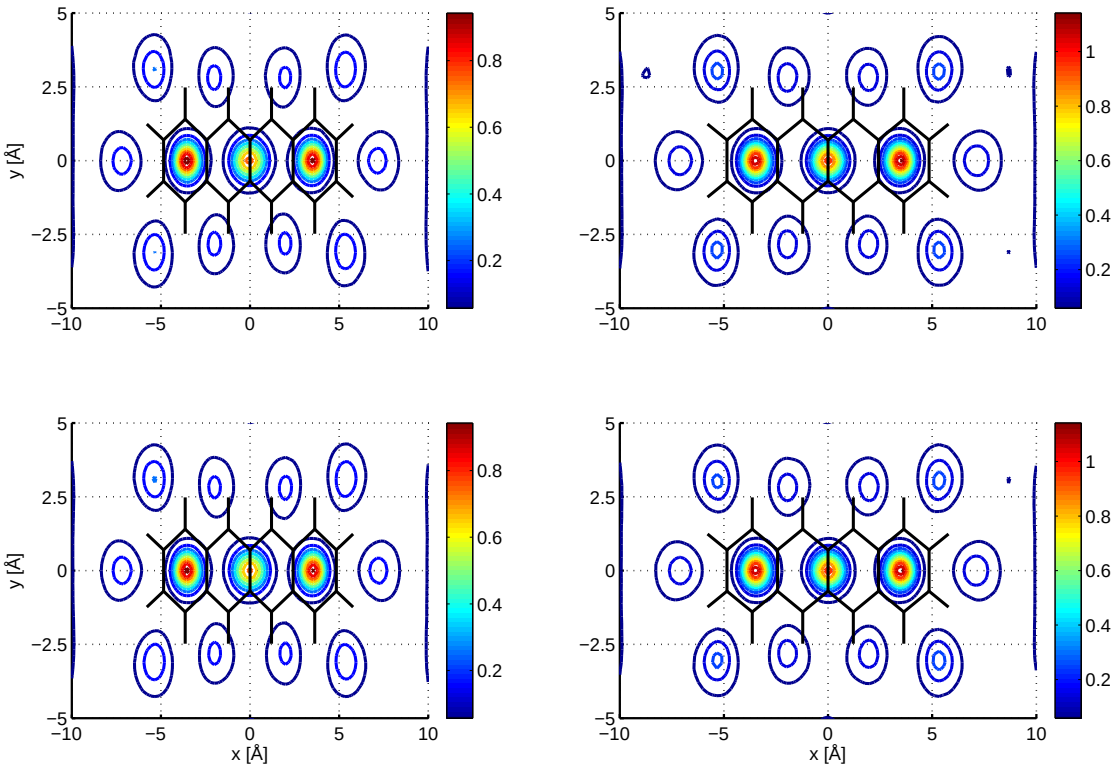

FIG. 11: Whitley *et al.* *The Journal of Chemical Physics*

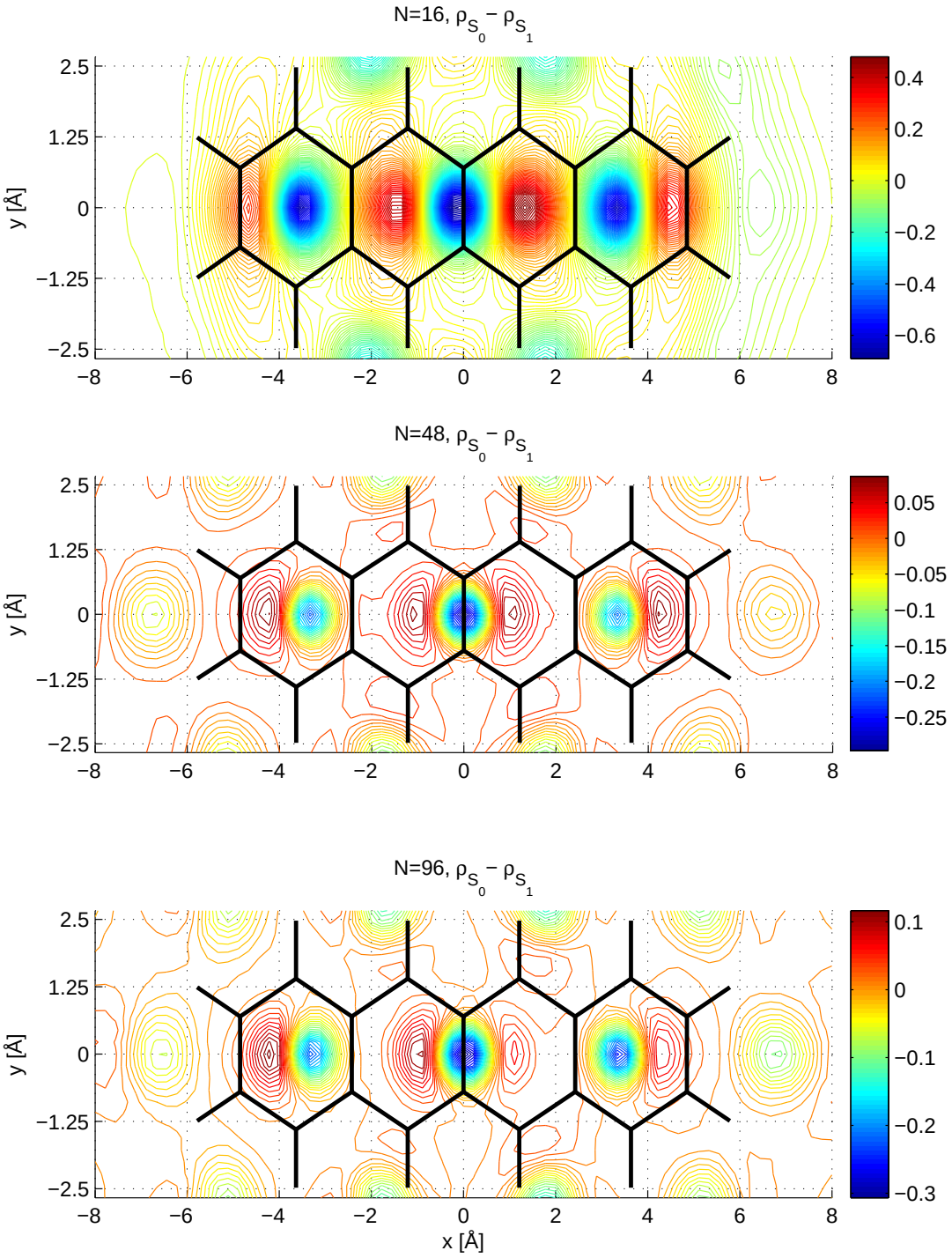

FIG. 12: Whitley *et al.* *The Journal of Chemical Physics*

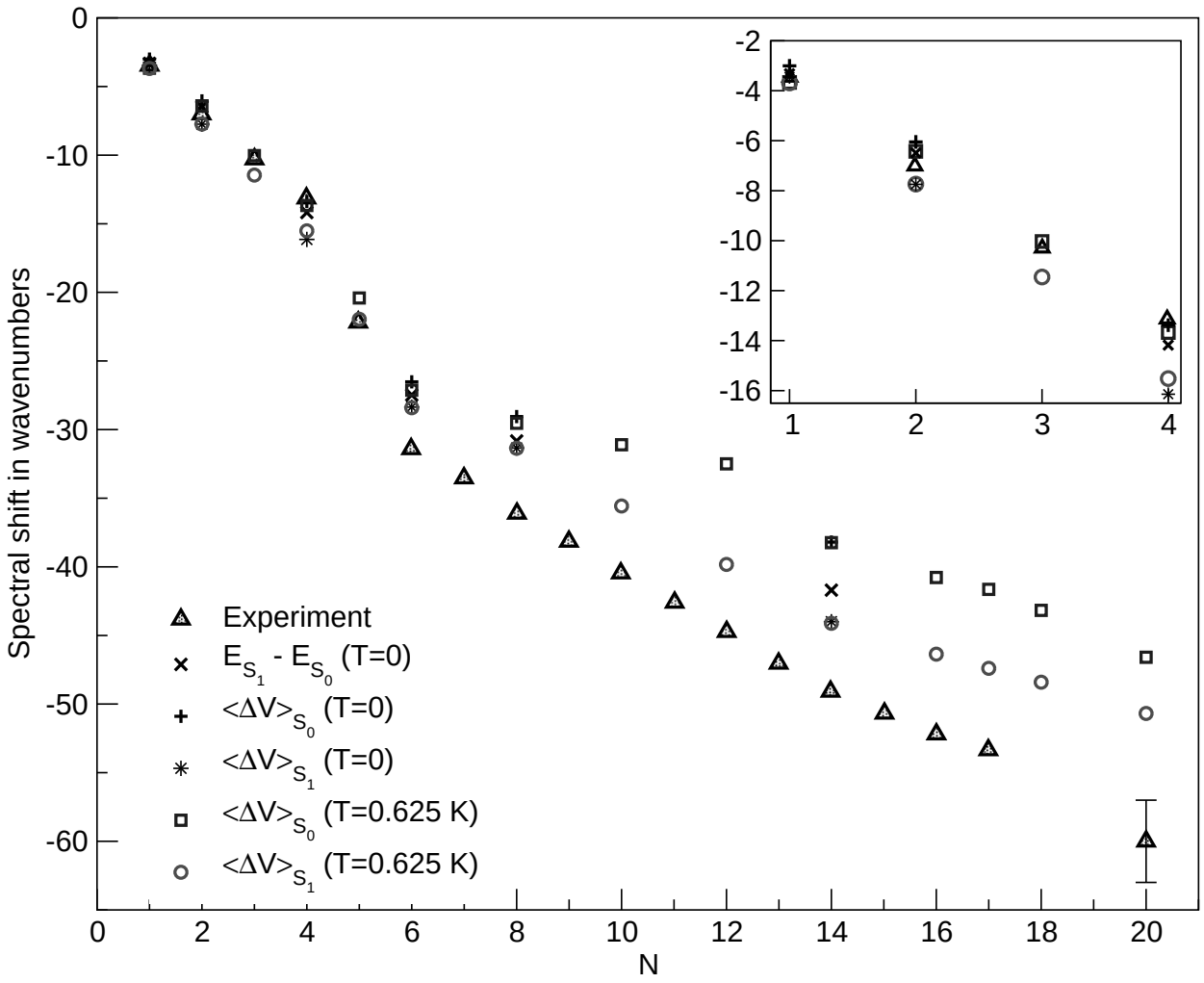

FIG. 13: Whitley *et al.* *The Journal of Chemical Physics*

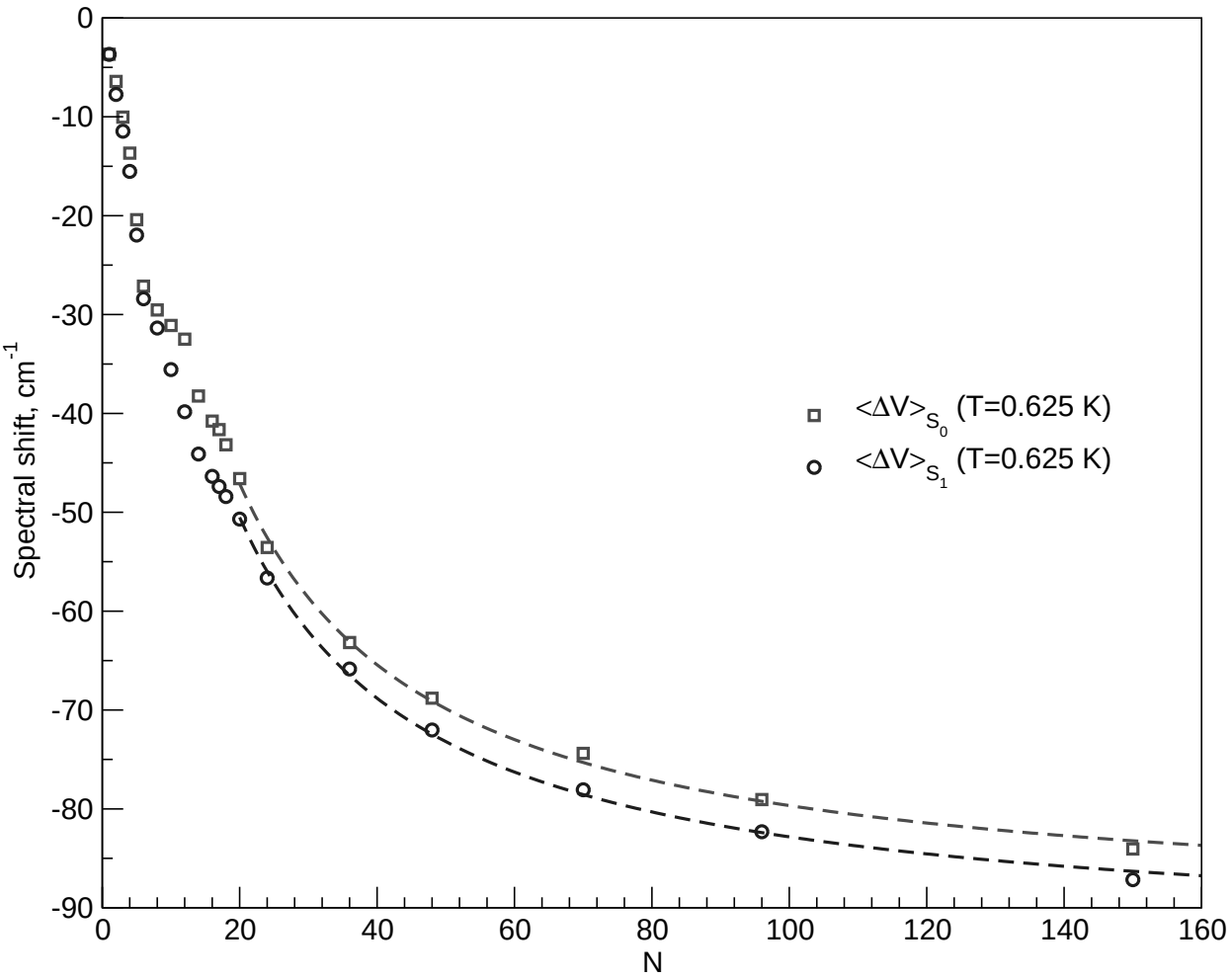

FIG. 14: Whitley *et al. The Journal of Chemical Physics*